HIGH ORDER POSITIVITY-PRESERVING DISCONTINUOUS GALERKIN METHODS FOR RADIATIVE TRANSFER EQUATIONS

DAMING YUAN[†], JUAN CHENG[‡], AND CHI-WANG SHU[§]

Abstract. The positivity-preserving property is an important and challenging issue for the numerical solution of radiative transfer equations. In the past few decades, different numerical techniques have been proposed to guarantee positivity of the radiative intensity in several schemes, however it is difficult to maintain both high order accuracy and positivity. The discontinuous Galerkin (DG) finite element method is a high order numerical method which is widely used to solve the neutron/photon transfer equations, due to its distinguished advantages such as high order accuracy, geometric flexibility, suitability for h- and p-adaptivity, parallel efficiency, and a good theoretical foundation for stability and error estimates. In this paper, we construct arbitrarily high order accurate DG schemes which preserve positivity of the radiative intensity in the simulation of both steady and unsteady radiative transfer equations in one- and two-dimensional geometry by using a combined technique of the scaling positivity-preserving limiter in [33] and a new rotational positivity-preserving limiter. This combined limiter is simple to implement and we prove the properties of positivity-preserving and high order accuracy rigorously. One- and two-dimensional numerical results are provided to verify the good properties of the positivity-preserving DG schemes.

Key words. positivity-preserving, high order accuracy, radiative transfer equation, discontinuous Galerkin (DG) scheme, discrete-ordinate method

AMS subject classifications. 65N30, 65N12, 65M60

1. Introduction.

The radiative transfer equation describes the interaction of photons with a scattering and absorbing background medium, which has wide applications in many areas such as astrophysics, inertial confinement fusion, optical molecular imaging, shielding, infrared and visible light in space and the atmosphere, just to name a few.

The radiative transfer equation is an integro-differential equation with six independent variables for a three spatial dimensional and time dependent problem. The high dimensionality and the presence of integral coupling terms bring a serious challenge to solve the equation numerically. Over the past few decades, several techniques for solving this kind of equations have been introduced, which include the Monte Carlo method, the discrete-ordinate method (DOM), the spherical harmonics method, the spectral method, the finite difference method, the finite volume method and the finite element method. Among these methods, the discrete-ordinate method has received particular attention in the literature due to its relatively high accuracy, flexibility, and relatively low computational cost. The discrete-ordinate method discretizes the solid angle with a set of ordinate directions. The integration over the solid angle that appears in the radiative transfer equation is evaluated by means of a weighted summation over the ordinate directions (numerical quadrature), where the specified weights are determined through algebraic and geometrical relationships [1, 8]. In this

[†]Institute of Applied Physics and Computational Mathematics, Beijing 100094, China and College of Mathematics and Information Science, Jiangxi Normal University, Nanchang, Jiangxi 330022, China. E-mail: damingyuan0915@163.com. Research is supported in part by NSFC grant 11261040. Additional support is provided by China Postdoctoral Science Foundation 2014M560918.

[‡]Institute of Applied Physics and Computational Mathematics, Beijing 100094, China. E-mail: cheng_juan@iapcm.ac.cn. Research is supported in part by NSFC grant 11471049.

[§]Division of Applied Mathematics, Brown University, Providence, RI 02912, U.S.A. E-mail: shu@dam.brown.edu. Research is supported in part by AFOSR grant F49550-12-1-0399 and NSF grant DMS-1418750.

paper, we focus on the discrete-ordinate discontinuous Galerkin method for solving the radiative transfer equation, which is among the most flexible numerical methods in discrete-ordinate formulations for the radiative transfer equation.

The discontinuous Galerkin (DG) finite element method was first introduced by Reed and Hill [27] in 1973 to solve the steady linear neutron transport (radiative transfer) equation, in which the numerical solution is allowed to be discontinuous across the cell boundaries. This feature makes the DG finite element method a local method, that is, it is possible to construct a set of small linear systems approximating the governing equation in each cell to avoid assembling and solving a large, global linear system. Soon after, in [15], theoretical properties of the DG method including stability and error estimates were provided. Later, Cockburn et al. [5, 4, 3, 6] established a framework to easily solve nonlinear time dependent problems, such as the compressible Euler equations of gas dynamics, using explicit, nonlinearly stable high order Runge-Kutta time discretizations [29] and DG discretization in space with exact or approximate Riemann solvers as interface fluxes and total variation bounded (TVB) nonlinear limiters [28] to achieve non-oscillatory properties for strong shocks. The DG method has many advantages such as high order accuracy, geometric flexibility, suitability for h- and p-adaptivity, extremely local data structure, high parallel efficiency and a good theoretical foundation for stability and error estimates. It is particularly powerful for convection-dominated problems, in which the solutions develop discontinuities or sharp fronts. The DG method has been widely used in many convection-dominated equations such as neutron/photon (radiative) transfer equation studied in this paper, Euler and Navier-Stokes equations for compressible gas dynamics, shallow water equations, KDV equations and so on.

In the transport community, second order DG method using piecewise linear polynomials has been employed predominantly to solve the discrete-ordinate transfer equation. Starting from the pioneering work [27] mentioned above, a piecewise linear function representation was used for three-dimensional unstructured tetrahedral meshes in [32, 24] and a trilinear representation was used for three-dimensional hexahedral meshes in [32]. In the neutron/photon transport area, limited research has been carried out using elements of higher polynomial degree, which include DG method up to order 4 developed for the steady transport equation by using hierarchical basis functions in [30, 21] and the quadratic DG method used for the neutron transport in spherical geometry [17, 23].

Robustness of numerical methods has attracted an increasing interest in the community of computational science. One mathematical aspect of robustness for numerical methods is the positivity-preserving property. It is known that under certain conditions, which are satisfied by almost all physical problems, the discrete-ordinate radiative transfer equations have nonnegative solutions whenever the source terms and the boundary conditions (and, for time-dependent problems, also the initial conditions) are nonnegative [7, 18]. For a good numerical method, it should ideally also yield a nonnegative solution. Especially in multidimensional problems, the appearance of negative solution could slow the convergence rate of the iterative processes, and sometimes may also cause a complete failure of convergence of the acceleration procedure. For time dependent problems, negative solution may lead to numerical instabilities. Furthermore, negative radiative intensity is a physically unrealistic solution which is difficult to be accepted by physicists.

A scheme for the radiative transfer equation is called positivity-preserving if it can always produce nonnegative solution for nonnegative source term and boundary

condition (and, for time dependent problems, also nonnegative initial condition). In this paper we use the word "positivity" loosely which is the same as nonnegativeness. Several studies exist in the literature on this issue, with various ways of ensuring positive intensities being proposed. The step scheme, which is the counterpart of the upwind scheme in computational fluid dynamics, is proved to be positivity-preserving but is only first order accurate and introduces excessive numerical smearing [2]. The diamond scheme reduces the numerical smearing, but negative intensities may appear. These negative intensities may be eliminated by using the negative intensity fix-up procedure, that is, setting them to zero. However, spatial oscillation and physically unrealistic intensities may still occur. The other existing positivity-preserving schemes include the variable-weight scheme which combines the step and the diamond schemes by a variable weight [10, 19], the linear exponential discontinuous finite-element method [31], the step and linear adaptive methods [22], the step characteristic scheme [12] and the linear characteristic scheme [11] which is nonnegative as long as the projected scattering source and projected outflow boundary fluxes remain positive which can be guaranteed by a rotational fix-up procedure. The positive intensities criteria for purely absorbing media is proposed by Fiveland in [9]. The linear discontinuous Galerkin finite-element method with the set-to-zero fix-up technique is proposed more recently in [20]. The procedures mentioned above are either only first or second order accurate, or use non-polynomial nonlinear procedures which require iterative procedures to obtain the solution even for the system inside each cell, or rely on the characteristic procedure and hence are difficult to be generalized to multi-dimensions.

For solving convection-dominated equations, such as Euler equations of compressible gas dynamics, recently Zhang and Shu developed a general framework which relies on a simple scaling limiter and can be applied to Runge-Kutta discontinuous Galerkin (RKDG) method and weighted essentially non-oscillatory (WENO) finite volume schemes of arbitrary order of accuracy on arbitrary meshes to ensure the positivity-preserving property without affecting the originally designed high order accuracy [33, 34, 35].

In this paper, we focus on designing a high order positivity-preserving DG method for solving the steady and unsteady discrete-ordinate radiative transfer equations in Cartesian coordinates. Differently from the explicit schemes for Euler equations and other convection dominated equations, the scheme we consider here is an implicit or iterative type, thus the above mentioned methodology of positivity-preserving scaling limiter proposed by Zhang and Shu can not be applied directly. In fact, if we adopt a similar positivity-preserving scaling limiter in the DG method for these radiative transfer equations, degeneracy of accuracy may happen for third and higher order schemes (see the Appendix of this paper). Here, instead, we develop a combined technique of the scaling positivity-preserving limiter and a rotational positivity-preserving limiter which can be used to solve the radiative transfer equations by implicit or iterative DG methods. This new limiter is simple to implement, does not affect convergence to weak solutions (Lax-Wendroff theorem), and can be theoretically proved to preserve positivity and to maintain the originally designed high order accuracy both in one and two spatial dimensions. One- and two-dimensional numerical tests for these positivity-preserving DG schemes are provided to demonstrate their effectiveness.

An outline of the rest of this paper is as follows. In Section 2, we describe the radiative transfer equation and its DG discretization for the steady and unsteady discrete-ordinate radiative transfer equation. In Section 3, we discuss the methodology

to construct positivity-preserving DG schemes for the radiative transfer equation in one spatial dimension. In Section 4, we present a positivity-preserving DG scheme in two spatial dimensions. In Section 5, numerical examples are given to demonstrate the good performance of these DG schemes. We give concluding remarks in Section 6.

2. The radiative transfer equation and its DG discretization.

2.1. The radiative transfer equation. The radiative transfer equation is the mathematical statement of the conservation of photons. The Eulerian derivation leads to the so-called integro-differential form of the radiative transfer equation. More details can be found in [25].

We first consider a steady-state, one-group, isotropically-scattering transfer equation

$$\mathbf{\Omega}\cdot\nabla_{\mathbf{r}}I(\mathbf{r},\mathbf{\Omega})+\sigma_t I(\mathbf{r},\mathbf{\Omega})=\frac{\sigma_s}{4\pi}\int_S I(\mathbf{r},\mathbf{\Omega})d\mathbf{\Omega}+q(\mathbf{r},\mathbf{\Omega}) \tag{2.1}$$

where $I(\mathbf{r},\mathbf{\Omega})$ is the radiative intensity in the direction $\mathbf{\Omega}$ and the spatial position $\mathbf{r}$, S is the unit sphere, $\sigma_s\geq 0$ is the scattering coefficient of the medium, σ_t is the extinction coefficient of the medium due to both absorption and scattering (that is, $\sigma_t\geq\sigma_s$), and $q(\mathbf{r},\mathbf{\Omega})$ is a given source term. For two spatial dimensional problems, the position vector $\mathbf{r}=(x,y)\in\mathcal{D}\subset\mathbb{R}^2$ and the vector $\mathbf{\Omega}$ is usually described by a polar angle β measured with respect to a fixed axis in space and a corresponding azimuthal angle φ. If we introduce $\mu=\cos\beta$, we may denote

$$d\mathbf{r}=dxdy,\qquad d\mathbf{\Omega}=\sin\beta d\beta d\varphi=-d\mu d\varphi.$$

To solve the radiative transfer equation numerically, we must discretize the spatial variables and the angular variables to obtain a system of simultaneous equations. In the discrete-ordinate method (DOM), the radiative transfer equation (2.1) is solved for a finite number of directions spanning the total solid angles of the unit sphere around a point in space, and integrals over solid angles are replaced by a numerical quadrature. For each discrete direction $\mathbf{\Omega}_{m,l}=(\zeta_m,\eta_l)$, $m=1,...,M$, $l=1,...,L$ where M,L are the numbers of directions in ζ and η respectively where $\zeta=\sin\beta\cos\varphi=\sqrt{1-\mu^2}\cos\varphi,\eta=\sin\beta\sin\varphi=\sqrt{1-\mu^2}\sin\varphi$. The equation (2.1) becomes a spatial differential equation which is written in Cartesian coordinates as

$$\zeta_m\frac{\partial I_{m,l}(\mathbf{r})}{\partial x}+\eta_l\frac{\partial I_{m,l}(\mathbf{r})}{\partial y}+\sigma_t I_{m,l}(\mathbf{r})=\frac{\sigma_s}{4\pi}\sum_{m',l'}\omega_{m',l'}I_{m',l'}(\mathbf{r})+q(\mathbf{r},\zeta_m,\eta_l), \tag{2.2}$$

where $I_{m,l}(\mathbf{r})=I(\mathbf{r},\zeta_m,\eta_l)$ is the radiative intensity in the direction (ζ_m,η_l), $\omega_{m,l}$ is the quadrature weight with $\sum_{m',l'}\omega_{m',l'}=4\pi$ (in this paper we assume $\omega_{m,l}>0$ for all m,l, which is correct for all the quadratures that we use in the numerical tests), and $\int_S I(\mathbf{r},\zeta,\eta)d\zeta d\eta\approx\sum_{m',l'}\omega_{m',l'}I(\mathbf{r},\zeta_{m'},\eta_{l'})$. In most applications of the DOM, S_N or T_N quadratures are used [13]. More details can be found in Section 5 when we give numerical examples.

2.1.1. The one-dimensional steady radiative transfer equation. The steady transfer equation in one-dimensional planar geometry can be described as follows,

$$\mu\frac{\partial I(x,\mu)}{\partial x}+\sigma_t I(x,\mu)=\frac{\sigma_s}{2}\int_{-1}^{+1}I(x,\mu)d\mu+q(x,\mu),\quad a\leq x\leq b,\ -1\leq\mu\leq 1, \tag{2.3}$$

where $I(x,\mu)$ is the radiative intensity in the direction μ and the spatial position x. The boundary condition for the equation (2.3) is specified as

$$I(a,\mu) = I^l(\mu),\ 0 < \mu \le 1; \qquad I(b,\mu) = I^r(\mu),\ \ -1 \le \mu < 0 \tag{2.4}$$

where I^l and I^r are the prescribed radiative intensity on the left and the right boundaries, respectively.

For each discrete direction m, one obtains a spatial differential equation as follows,

$$\mu_m \frac{\partial I_m(x)}{\partial x} + \sigma_t I_m(x) = \frac{\sigma_s}{2} \sum_{m'=1}^{M} \omega_{m'} I_{m'}(x) + q_m(x), \qquad m = 1, ..., M \tag{2.5}$$

where M is the number of directions, μ_m is the direction cosines along the x-coordinate of the direction m, $\omega_m > 0$ is the quadrature weight with $\sum_m \omega_m = 2$ and $I_m(x) = I(x,\mu_m)$ is the radiative intensity in the direction m. $\int_{-1}^{+1} I(x,\mu)d\mu \approx \sum_{m'=1}^{M} \omega_{m'} I_{m'}(x)$.

2.1.2. The one-dimensional unsteady radiative transfer equation. We assume the range of the time variable as $0 < t \le T$, then the unsteady isotropically-scattering transport problem in planar geometry is described as follows,

$$\begin{aligned} &\frac{1}{c}\frac{\partial I(x,\mu,t)}{\partial t} + \mu \frac{\partial I(x,\mu,t)}{\partial x} + \sigma_t I(x,\mu,t) = \frac{\sigma_s}{2}\int_{-1}^{+1} I(x,\mu,t)d\mu + q(x,\mu,t), \\ &\qquad\qquad a \le x \le b,\ \ -1 \le \mu \le 1,\ 0 < t \le T, \end{aligned} \tag{2.6}$$

where c is the speed of photon.

For the above unsteady radiative transfer equation, we need to specify the boundary condition as

$$I(a,\mu,t) = I^l(\mu,t),\ 0 < \mu \le 1,\ 0 \le t \le T;\ I(b,\mu,t) = I^r(\mu,t),\ -1 \le \mu < 0,\ 0 \le t \le T \tag{2.7}$$

and the initial condition as

$$I(x,\mu,0) = I_0(x,\mu). \tag{2.8}$$

Similarly, the discrete-ordinate approximation for the unsteady radiative transfer equation in planar geometry can be written as

$$\frac{1}{c}\frac{\partial I_m(x,t)}{\partial t} + \mu_m \frac{\partial I_m(x,t)}{\partial x} + \sigma_t I_m(x,t) = \frac{\sigma_s}{2} \sum_{m'=1}^{M} \omega_{m'} I_{m'}(x,t) + q_m(x,t), \quad m = 1, ..., M. \tag{2.9}$$

2.2. The DG method for the discrete-ordinate radiative transfer equation. In this paper, we employ the DG method to discretize the spatial variables of the discrete-ordinate radiative transfer equations. Here we first take the one-dimensional radiative transfer equation as an example to show the form of the DG discretization for this kind of equations. The specific form of the DG scheme for the two-dimensional radiative transfer equation will be given in Section 4.

Without loss of generality, we denote $S_i = [x_{i-1/2}, x_{i+1/2}]$ $(i = 1, \cdots, N_x)$ as a subdivision of $[a,b]$ with $a = x_{1/2} < x_{3/2} < \cdots < x_{N_x+1/2} = b$, $\Delta x_i = x_{i+1/2} - x_{i-1/2}$ and $h = \max_{1 \le i \le N_x}(\Delta x_i)$.

We define the finite-element space consisting of the following piecewise polynomials

$$V_h^k = \{I_m^h(x) \in L^2(a,b) : I_m^h(x)|_{S_i} = I_{m,i}(x) \in P^k(S_i), \forall S_i, i = 1, \cdots, N_x\}$$

where $P^k(S_i)$ denotes the set of polynomials of degree up to k defined in the cell S_i. It is noted that functions in V_h^k may be discontinuous across cell boundaries.

Due to the discontinuous nature of the spatial approximation, functions $I_m^h(x) \in V_h^k$ are double-valued at interior nodes (cell boundaries) $x_{i+1/2}$ for $i = 2, \cdots, N_x - 1$. Consider a node $x_{i+1/2}$ separating two cells S_i and S_{i+1}. For the convenience of the following discussion, we will use the notation $I_{m,i}(x)$ to denote the polynomial solution of I_m^h inside the cell S_i. The left and right values of $I_m^h(x)$ at the node $x_{i+1/2}$ are therefore given by

$$I_m^h(x_{i+1/2}^-) = I_{m,i}(x_{i+1/2}), \qquad I_m^h(x_{i+1/2}^+) = I_{m,i+1}(x_{i+1/2}), \tag{2.10}$$

respectively.

2.2.1. The DG method for the one-dimensional steady radiative transfer equation. We consider a given direction μ_m, and only illustrate the case of $\mu_m > 0$, as a similar procedure can be repeated for $\mu_m < 0$. By applying the upwind principle to determine the numerical flux at the cell boundaries, the DG method for solving (2.5) is defined as follows: find the unique function $I_m^h(x) \in V_h^k$ such that, for all the test functions $b^h(x) \in V_h^k$ where $b^h(x)|_{S_i} = b_i(x) \in P^k(S_i), \forall S_i, i = 1, \cdots, N_x$, we have

$$\begin{aligned} &\int_{S_i} (-\mu_m I_m^h(x)(b^h)'(x) + \sigma_t I_m^h(x) b^h(x))dx + \mu_m I_m^h(x_{i+1/2}^-) b^h(x_{i+1/2}^-) = \\ &\int_{S_i} \tfrac{\sigma_s}{2} \phi_i(x) b^h(x) dx + \int_{S_i} q_m(x) b^h(x) dx + \mu_m I_m^h(x_{i-1/2}^-) b^h(x_{i-1/2}^+), \end{aligned}$$

i.e.

$$\begin{aligned} &\int_{S_i} (-\mu_m I_{m,i}(x) b_i'(x) + \sigma_t I_{m,i}(x) b_i(x))dx + \mu_m I_{m,i}(x_{i+1/2}) b_i(x_{i+1/2}) = \\ &\int_{S_i} \tfrac{\sigma_s}{2} \phi_i(x) b_i(x) dx + \int_{S_i} q_m(x) b_i(x) dx + \mu_m I_{m,i-1}(x_{i-1/2}) b_i(x_{i-1/2}) \end{aligned} \tag{2.11}$$

where

$$\phi_i(x) = \sum_{m'=1}^{M} \omega_{m'} I_{m',i}(x). \tag{2.12}$$

2.2.2. The DG method for the unsteady radiative transfer equation. The DG method, with backward Euler time discretization, for solving the unsteady DOM transfer equation (2.9) is similar to the steady state scheme (2.11). When the n-th time step solution $I_{m,i}^n(x)$ (for all $m = 1, \cdots, M$ and $i = 1, \cdots, N_x$) is known, we would like to find polynomials $I_{m,i}^{n+1}(x) \in P^k(S_i)$, for all $m = 1, \cdots, M$ and $i = 1, \cdots, N_x$, such that

$$\begin{aligned} &\int_{S_i} (-\mu_m I_{m,i}^{n+1}(x) b_i'(x) + \tilde{\sigma}_t I_{m,i}^{n+1}(x) b_i(x))dx + \mu_m I_{m,i}^{n+1}(x_{i+1/2}) b_i(x_{i+1/2}) = \\ &\int_{S_i} \tfrac{\sigma_s}{2} \phi_i^{n+1}(x) b_i(x) dx + \int_{S_i} \tilde{q}_{m,i}(x) b_i(x) dx + \mu_m I_{m,i-1}^{n+1}(x_{i-1/2}) b_i(x_{i-1/2}) \end{aligned} \tag{2.13}$$

where $\tilde{\sigma}_t = \sigma_t + \frac{1}{c\Delta t^n}$, $\tilde{q}_{m,i}(x) = q_m(x, t^{n+1}) + \frac{1}{c\Delta t^n} I_{m,i}^n(x)$, and $\Delta t^n = t^{n+1} - t^n$ is the time step size. We use backward Euler in order to avoid the extreme constraint on the time step for explicit time stepping due to the high speed c. Of course, higher order implicit time stepping methods can also be used, but our discussion in this paper is restricted to first order backward Euler time stepping.

2.3. The solution algorithm for the DG method. The discrete set of algebraic equations in the DOM-DG schemes such as (2.11) and (2.13) is usually solved by an iteration method in an optimal sweeping order. This is usually referred to as the grid sweeping algorithm. For a specific discrete direction, the optimal marching procedure starts from a cell located at a corner of the computational domain. We determine the corner where the calculation begins for each specific discrete direction by the sign of the direction cosines such as μ_m for one-dimensional problems and (ζ_m, η_l) for two-dimensional problems under consideration in a way that the upstream cell boundaries lie on the boundary of the domain. For example, when $\zeta_m > 0,\ \eta_l > 0$, the sweeping starts from the bottom-left corner cell, whose left and bottom cell boundaries coincide with the inflow boundary of the domain where the intensity function is prescribed. The discrete equations for all the remaining cells are solved successively in the direction of the orientation of the direction cosines, so that the intensities at the upstream boundaries of the cell we are computing can be obtained either from the boundary conditions or from the calculations performed in the previously computed cells. Without the coupling integral terms, this marching procedure provides the DG solution in all cells just in one sweep, which is a major advantage of the DG methods. For iterative methods used to solve the discretized transfer equation with the coupling integral terms, one of the widely used methods is the so-called source iteration (SI) method [16], which is defined for solving the DG scheme (2.11)-(2.12) as follows: When the ℓ-th iteration solution $I_{m,i}^{(\ell)}$ (for all $m = 1, \cdots, M$ and $i = 1, \cdots, N_x$) is known, we compute $I_{m,i}^{(\ell+1)}$, for $i = 1, \cdots, N_x$ (in this order when $\mu > 0$), and for each fixed i, running through $m = 1, \cdots, M$ to solve

(2.14)
$$\begin{aligned}&\int_{S_i}(-\mu_m I_{m,i}^{(\ell+1)}(x)b_i'(x) + \sigma_t I_{m,i}^{(\ell+1)}(x)b_i(x))dx + \mu_m I_{m,i}^{(\ell+1)}(x_{i+1/2})b_i(x_{i+1/2})\\ &= \int_{S_i}\tfrac{\sigma_s}{2}\phi_i^{(*)}(x)b_i(x)dx + \int_{S_i} q_m(x)b_i(x)dx + \mu_m I_{m,i-1}^{(\ell+1)}(x_{i-1/2})b_i(x_{i-1/2})\end{aligned}$$

with

$$\phi_i^{(*)}(x) = \sum_{m'=1,\cdots,M} \omega_{m'} I_{m',i}^{(*)}(x) \tag{2.15}$$

where $I_{m',i}^{(*)}(x)$ is taken as $I_{m',i}^{(\ell+1)}(x)$ if it is already available, otherwise it is taken as $I_{m',i}^{(\ell)}(x)$. Since $I_{m,i-1}^{(\ell+1)}(x_{i-1/2})$ (for $i = 1$ this is taken as the given boundary condition) and the other $(\ell+1)$-th iteration solution needed on the right hand side of (2.14) have already been computed in the sweep, the SI solver (2.14) is completely local in cell S_i, thus can be very efficiently computed. The initial iteration values $I_{m,i}^{(0)}$ can be determined arbitrarily (e.g. by the boundary conditions). The source iteration process continues until a prescribed convergence criterion is satisfied, in our numerical experiments this is taken as when the maximum residue is less than 10^{-14}. In the SI method, each ordinate is solved independently while the couplings between different ordinates are deferred to the integral term involving $\phi_i^{(*)}(x)$, which uses a mixture of information from both $(\ell+1)$-th (when available) and ℓ-th iterations.

Similarly, the SI method solving the DG scheme for the unsteady radiative transfer equation (2.13) can be described as follows

(2.16)
$$\begin{aligned}&\int_{S_i}(-\mu_m I_{m,i}^{n+1,(\ell+1)}(x)b_i'(x) + \tilde{\sigma}_t I_{m,i}^{n+1,(\ell+1)}(x)b_i(x))dx + \mu_m I_{m,i}^{n+1,(\ell+1)}(x_{i+1/2})b_i(x_{i+1/2})\\ &= \int_{S_i}\tfrac{\sigma_s}{2}\phi_i^{n+1,(*)}(x)b_i(x)dx + \int_{S_i}\tilde{q}_{m,i}(x)b_i(x)dx + \mu_m I_{m,i-1}^{n+1,(\ell+1)}(x_{i-1/2})b_i(x_{i-1/2}).\end{aligned}$$

3. High order positivity-preserving DG scheme for the discrete-ordinate radiative transfer equation in one spatial dimension. Generally, higher order approximations for radiative intensity may provide more accurate solutions but artifacts might appear such as negativeness of the solutions. In this section, we first discuss how to design a high order positivity-preserving DG scheme for both the steady radiative transfer equation and the unsteady radiative transfer equation in one spatial dimension. In the next section, we will propose a high order positivity-preserving DG scheme for the two-dimensional radiative transfer equation.

3.1. High order positivity-preserving DG scheme for the one-dimensional steady discrete-ordinate radiative transfer equation. We denote

$$G_i = \{x_{i-1/2} = \hat{x}_i^1, \hat{x}_i^2, \cdots, \hat{x}_i^{N-1}, \hat{x}_i^N = x_{i+1/2}\}$$

as the N-point Gauss-Lobatto quadrature points in the cell S_i and $\hat{w}_\alpha > 0$ ($\alpha = 1, 2, \cdots, N$) as the corresponding quadrature weights, where N could be chosen as the smallest integer satisfying $2N - 3 \geq k$. However, in this paper, in order to make the rotational limiter simpler, we choose $N = k + 1$ so that the k-th degree polynomial solution can be completely and uniquely determined by its values at these Gauss-Lobatto points. For a polynomial $I_{m,i}(x)$, denote by $\bar{I}_{m,i}$ its cell average in S_i (from now on, we denote by $\bar{f}$ the cell average of the function f), then we have

$$\bar{I}_{m,i} = \frac{1}{\Delta x_i} \int_{S_i} I_{m,i}(x)dx = \sum_{\alpha=1}^{N} \hat{w}_\alpha I_{m,i}(\hat{x}_i^\alpha).$$

We aim to develop a high order positivity-preserving DG scheme for solving the discrete-ordinate steady radiative transfer equation (2.5). That is, if we know the source term, the values of I at the domain boundary, $\{I_{m,i'}^{(\ell)}(\hat{x}_{i'}^\alpha), \forall \alpha, m, i'\}$ and $\{I_{m,i'}^{(\ell+1)}(\hat{x}_{i'}^\alpha), \alpha = 1, \cdots, N\}$ in all the upstream cells of the cell S_i are nonnegative, then we would like to "limit" the DG solution $I_{m,i}^{(\ell+1)}(x)$ computed by (2.14) to obtain a new polynomial $\hat{I}_{m,i}^{(\ell+1)}(x)$ such that $\hat{I}_{m,i}^{(\ell+1)}(\hat{x}_i^\alpha)$ are nonnegative for all $\alpha = 1, \cdots, N$. This of course also implies that the cell average of $\hat{I}_{m,i}(x)$ is nonnegative. Furthermore, the limiting procedure should not affect the accuracy of the scheme, i.e., $|\hat{I}_{m,i}^{(\ell+1)}(x) - I_{m,i}^{(\ell+1)}(x)| \leq \mathcal{C}h^{k+1}$ when the exact solution is smooth. Here and below, $\mathcal{C}$ is a constant independent of h, which may take different values in different locations. After the limited polynomial $\hat{I}_{m,i}(x)$ is obtained, it will be relabeled as $I_{m,i}^{(\ell+1)}(x)$ before moving to the next direction $m + 1$ or to the next cell, i.e. S_{i+1} for the case $\mu_m > 0$.

Consider again the case of $\mu_m > 0$. If we take the test function $b_i(x) = 1$ in (2.14), then we obtain

$$\sigma_t \int_{S_i} I_{m,i}^{(\ell+1)}(x)dx + \mu_m I_{m,i}^{(\ell+1)}(x_{i+1/2}) = \frac{\sigma_s}{2} \int_{S_i} \phi_i^{(*)}(x)dx + \int_{S_i} q_m(x)dx + \mu_m I_{m,i-1}^{(\ell+1)}(x_{i-1/2}),$$

i.e.,

$$\sigma_t \bar{I}_{m,i}^{(\ell+1)} \Delta x_i + \mu_m I_{m,i}^{(\ell+1)}(x_{i+1/2}) = \frac{\sigma_s}{2} \bar{\phi}_i^{(*)} \Delta x_i + \bar{q}_{m,i} \Delta x_i + \mu_m I_{m,i-1}^{(\ell+1)}(x_{i-1/2}). \tag{3.1}$$

From the above assumption, we know $\bar{q}_{m,i} \geq 0$, $\bar{\phi}_i^{(*)} \geq 0$ and $I_{m,i-1}^{(\ell+1)}(x_{i-1/2}) \geq 0$, then by (3.1) and the mean value theorem, there exists $\xi \in [x_{i-\frac{1}{2}}, x_{i+\frac{1}{2}}]$ so that the

following inequality is satisfied,

$$I_{m,i}^{(\ell+1)}(\xi) = \frac{\mu_m}{\mu_m + \sigma_t \Delta x_i} I_{m,i}^{(\ell+1)}(x_{i+\frac{1}{2}}) + \frac{\sigma_t \Delta x_i}{\mu_m + \sigma_t \Delta x_i} \bar{I}_{m,i}^{(\ell+1)} \geq 0. \tag{3.2}$$

Thus it is also easy to see that at least one of $I_{m,i}^{(\ell+1)}(x_{i+\frac{1}{2}})$ and $\bar{I}_{m,i}^{(\ell+1)}$ is nonnegative.

We remark that (3.2) states that the original DG solution obtained by (2.14), without being limited yet, is nonnegative at least at one point in the cell. This is crucial for the success of the limiter to be introduced later. In the work of Zhang and Shu [33, 35], the original DG solution has a nonnegative cell average, then a simple scaling limiter can be applied to bring the whole polynomial at the desired Gauss-Lobatto points to be nonnegative, without sacrificing the original high order accuracy. An obvious idea here would be to adopt a similar scaling limiter, which can be described as follows,

$$\hat{I}_{m,i}^{(\ell+1)}(x) = \lambda(I_{m,i}^{(\ell+1)}(x) - I_{m,i}^{(\ell+1)}(\xi)) + I_{m,i}^{(\ell+1)}(\xi), \tag{3.3}$$

where

$$\lambda = \min\left\{ \left| \frac{I_{m,i}^{(\ell+1)}(\xi)}{I_{m,i}^{(\ell+1)}(\xi) - z_i} \right|, 1 \right\}, \qquad z_i = \min_{\alpha=1,\ldots,N}(0, I_{m,i}^{(\ell+1)}(\hat{x}_i^\alpha)).$$

Then we can easily verify that $\hat{I}_{m,i}^{(\ell+1)}(\hat{x}_i^\alpha) \geq 0, \alpha = 1, \cdots, N$ and therefore also $\bar{\hat{I}}_{m,i}^{(\ell+1)} = \frac{1}{\Delta x_i} \int_{S_i} \hat{I}_{m,i}^{(\ell+1)}(x)dx = \sum_{\alpha=1}^N \hat{w}_\alpha \hat{I}_{m,i}^{(\ell+1)}(\hat{x}_i^\alpha) \geq 0$. This is exactly the scaling limiter used in Zhang and Shu [33, 35], with the cell average $\bar{I}_{m,i}^{(\ell+1)}$ replaced by $I_{m,i}^{(\ell+1)}(\xi)$. This appears to be just a small change, as both $\bar{I}_{m,i}^{(\ell+1)}$ and $I_{m,i}^{(\ell+1)}(\xi)$ are particular point values of the DG polynomial solution $I_{m,i}^{(\ell+1)}(x)$ at different points inside the cell S_i. It is proved in [33, 35] that the scaling limiter with $\bar{I}_{m,i}^{(\ell+1)}$ maintains the original high order accuracy. Unfortunately, the same scaling limiter (3.3) with $I_{m,i}^{(\ell+1)}(\xi)$ defined by (3.2) can only guarantee the original second order accuracy for the piecewise linear $k = 1$ case, but may lead to possible degeneracy of the original high order accuracy for $k \geq 2$. For a more detailed discussion on this issue, we refer to the appendix of this paper.

In order to keep the high order accuracy of the method as well as the positivity-preserving property of the radiative intensity, we adopt an alternative positivity-preserving limiter which will be illustrated in the following subsections. As shown above, at least one of $\bar{I}_{m,i}^{(\ell+1)}$ and $I_{m,i}^{(\ell+1)}(x_{i+\frac{1}{2}})$ is non-negative. The limiting strategy depends on which one is non-negative. If $\bar{I}_{m,i}^{(\ell+1)} \geq 0$, then the same scaling limiter as introduced in [33, 35] is employed which will be introduced in subsection 3.1.1, otherwise a rotational limiter is applied which will be described in subsection 3.1.2.

3.1.1. The scaling limiter. If $\bar{I}_{m,i}^{(\ell+1)} \geq 0$, we apply the scaling limiter [33] to modify $I_{m,i}^{(\ell+1)}(x)$ as follows

$$\hat{I}_{m,i}^{(\ell+1)}(x) = \lambda(I_{m,i}^{(\ell+1)}(x) - \bar{I}_{m,i}^{(\ell+1)}) + \bar{I}_{m,i}^{(\ell+1)} \tag{3.4}$$

with

$$\lambda = \min\left\{ \left| \frac{\bar{I}_{m,i}^{(\ell+1)}}{\bar{I}_{m,i}^{(\ell+1)} - z_i} \right|, 1 \right\}, \qquad z_i = \min_{\alpha=1,\ldots,N}(0, I_{m,i}^{(\ell+1)}(\hat{x}_i^\alpha)). \tag{3.5}$$

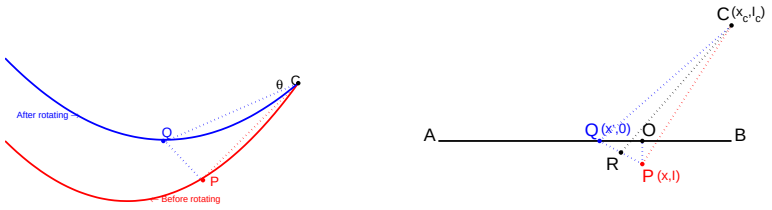

FIG. 3.1. *Left: The rotational transformation; Right: Sketch for the rotation.*

This scaling limiter can keep the original high order of accuracy of the unlimited polynomial, as proved in [33]. Here we only state the conclusion in the following proposition.

Proposition 1. *(Zhang and Shu [33]) Assume $I_{m,i}^{(\ell+1)}(x)$ is a k-th degree polynomial defined on cell S_i which approximates a smooth function $I(x) \geq 0$ to $(k+1)$-th order accuracy, and $\bar{I}_{m,i}^{(\ell+1)} \geq 0$, then the limited polynomial $\hat{I}_{m,i}^{(\ell+1)}(x)$ defined by (3.4) and (3.5) achieves positivity $\hat{I}_{m,i}^{(\ell+1)}(\hat{x}_i^{\alpha}) \geq 0$ for $\alpha = 1, ..., N$ and maintains the same $(k+1)$-th order accuracy for approximating $I(x)$.*

3.1.2. The rotational limiter. First, we recall a few notations about the rotational transformation. For simplicity of notations, we denote the end point $x_{i+1/2}$ as x_c and $I_{m,i}(x_{i+1/2})$ as I_c. Similarly, for any points $x, x^{'} \in S_i$, the values of the radiative intensity at these points are denoted as I and I' respectively. As shown in Figure 3.1 (left), let the point $P(x, I)$ be rotated clockwise for an angle θ around the point $C(x_c, I_c)$, which is called the center of rotation, and reach the point $Q(x^{'}, I')$. We also denote AB as the line segment between the points A and B and $|AB|$ as the Euclidean length of AB, respectively.

The rotational transformation can be written as a vector multiplied by a matrix calculated from the angle θ as follows,

$$\begin{bmatrix} I' \\ x^{'} \end{bmatrix} = \mathbf{M} \begin{bmatrix} I - I_c \\ x - x_c \end{bmatrix} + \begin{bmatrix} I_c \\ x_c \end{bmatrix} \tag{3.6}$$

where the rotational matrix $\mathbf{M}$ is defined as $\begin{bmatrix} \cos\theta & \sin\theta \\ -\sin\theta & \cos\theta \end{bmatrix}$.

Suppose $I' = 0$, then it is easy to verify that the value of θ can be computed by the following formula

$$\theta = \arccos \frac{2a^2 - b^2}{2a^2}, \tag{3.7}$$

where $a^2 = (x_c - x)^2 + (I_c - I)^2$ and

$$b^2 = (x_c - \sqrt{a^2 - I_c^2} - x)^2 + I^2.$$

Now, just like in the scaling limiter case, we assume $I_{m,i}(x)$ is a k-th degree polynomial defined in the cell S_i which approximates a smooth function $I(x) \geq 0$ to $(k+1)$-th order accuracy, and $I_{m,i}(x_{i+1/2}) \geq 0$. We would like to obtain a limited

polynomial $\hat{I}_{m,i}(x)$ with rotation, such that $\hat{I}_{m,i}(\hat{x}_i^\alpha) \geq 0$ for $\alpha = 1, ..., N$, while maintaining the same $(k+1)$-th order accuracy for approximating $I(x)$. For the convenience of description, we call $\hat{x}_i^\alpha$ to be a negative Gauss-Lobatto point if $I_{m,i}(\hat{x}_i^\alpha) < 0$.

The rotational limiter algorithm:

1. For each negative Gauss-Lobatto point $\hat{x}_i^\alpha$ in the cell S_i, compute the rotational angle $\theta_{m,i}^\alpha$ by (3.7) so that the point $(\hat{x}_i^\alpha, I_{m,i}(\hat{x}_i^\alpha))$ is rotated around $(\hat{x}_i^N, I_{m,i}(\hat{x}_i^N))$ clockwise to reach the new point $(\hat{x}_i^{'\alpha}, 0)$. If a particular $\hat{x}_i^\alpha$ is not a negative Gauss-Lobatto point, then we set $\theta_{m,i}^\alpha = 0$.
2. Taking $\theta_{m,i} = \max_{\alpha=1,\cdots,N-1} \theta_{m,i}^\alpha$, we rotate the polynomial $I_{m,i}(x)$ to obtain $\check{I}_{m,i}(x)$ by the rotational transformation (3.6) with $\theta = \theta_{m,i}$. Then it is easy to see that $\check{I}_{m,i}(\hat{x}_i^{'\alpha}) \geq 0$ for all $\alpha = 1, ..., N-1$.
3. The final modified polynomial $\hat{I}_{m,i}(x)$ is the interpolation polynomial at all the $N = k+1$ Gauss-Lobatto points which are determined by $\hat{I}_{m,i}(\hat{x}_i^\alpha) = \check{I}_{m,i}(\hat{x}_i^{'\alpha})$, $\alpha = 1, \cdots, N-1$ and $\hat{I}_{m,i}(\hat{x}_i^N) = I_{m,i}(\hat{x}_i^N)$.

From the definition of the rotational limiter, we can clearly see that $\hat{I}_{m,i}(\hat{x}_i^\alpha) \geq 0$ for all $\alpha = 1, ..., N$. That is,

Proposition 2. *$\hat{I}_{m,i}(\hat{x}_i^\alpha)$ is nonnegative for all $\alpha = 1, \cdots, N$, i.e., the rotational limiter is positivity-preserving.*

Next we will show that the above described rotational limiter can maintain the original high order accuracy. First we introduce the following lemma.

Lemma 1. *Suppose the k-th degree polynomial $I_h(x)$ is a $(k+1)$-order accurate approximation of the smooth function $I(x)$ in the cell S_i. As shown in Figure 3.1 (right), assume the Gauss-Lobatto point $P(x, I)$ with $I < 0$ (here $I = I_h(x)$ is a short notation) in the interval AB rotates clockwise by angle θ ($\angle PCQ = \theta$), around the point $C(x_c, I_c)$ with $I_c > 0$ to reach the point $Q(x^{'}, 0)$. Suppose $|AB| = h$ ($A = x_{i-1/2}$, $B = x_{i+1/2}$), then we have*

$$\tan\frac{\theta}{2} \leq \mathcal{C}h^k \tag{3.8}$$

Proof: Suppose the point O is the foot of the perpendicular projection of P to AB. We first show that $|OQ| \leq \mathcal{C}h^{k+1}$. Let $x = \hat{x}_i^\alpha$ be one of the Gauss-Lobatto points in the interval AB, then $|OB| = |x_c - x| \geq \mathcal{C}_1 h$, for example $\mathcal{C}_1 \approx 0.35$ if $N = 5$.

An essential observation is that

$$|BQ| = \sqrt{|CQ|^2 - |CB|^2} = \sqrt{|CP|^2 - |CB|^2} = \sqrt{(x_c - x)^2 + (I_c - I)^2 - I_c^2}$$

and $|OQ| = |BQ| - |OB|$, then

$$|OQ| = |I|\frac{|I - 2I_c|}{\sqrt{(x_c - x)^2 + (I_c - I)^2 - I_c^2} + (x_c - x)}. \tag{3.9}$$

Since $I_c > 0, I < 0$, we have, for constants $\mathcal{C}_0$, $\mathcal{C}_2 > 0$,

$$\begin{aligned} I_c \leq |I_c - I| &= |I_h(x_c) - I_h(x)| \\ &\leq |I_h(x_c) - I(x_c)| + |I(x_c) - I(x)| + |I(x) - I_h(x)| \\ &\leq \mathcal{C}_0 h^{k+1} + \frac{dI}{dx}(\xi)(x_c - x) \leq \mathcal{C}_2 h \end{aligned}$$

where $\xi \in [x, x_c]$. Also, since $I = I_h(x) < 0$ and $I(x) \geq 0$, we have $|I| \leq |I - I(x)| = |I_h(x) - I(x)| \leq \mathcal{C}_3 h^{k+1}$ for some constant $\mathcal{C}_3$. Therefore, the numerator of the coefficient to I on the right side of (3.9) satisfies

$$|I - 2I_c| \leq |I| + 2|I_c| \leq \mathcal{C}_4 h$$

and the denominator of the coefficient to I on the right side of (3.9) satisfies

$$\sqrt{(x_c - x)^2 + (I_c - I)^2 - I_c^2} + (x_c - x) \geq x_c - x \geq \mathcal{C}_1 h$$

Hence the coefficient itself is bounded by a constant $\mathcal{C}_5$, which, by (3.9), implies

$$|OQ| \leq \mathcal{C}_6 h^{k+1}$$

where $\mathcal{C}_6 = \mathcal{C}_3\mathcal{C}_5$.

It remains to show that $\tan\frac{\theta}{2} \leq \mathcal{C}h^k$. Let the point R be the midpoint of PQ as shown in Figure 3.1 (right). Since $|OQ| \leq \mathcal{C}_6 h^{k+1}$ and $|PO| = |I| \leq \mathcal{C}_3 h^{k+1}$, we have $|PR| \leq \mathcal{C}_7 h^{k+1}$ where $\mathcal{C}_7 = \frac{1}{2}\sqrt{(\mathcal{C}_3)^2 + (\mathcal{C}_6)^2}$. Then

$$\tan\frac{\theta}{2} = \frac{|PR|}{|RC|} < \frac{|PR|}{|OB|} \leq \frac{\mathcal{C}_7 h^{k+1}}{\mathcal{C}_1 h} \leq \mathcal{C}h^k,$$

where $\mathcal{C} = \mathcal{C}_7/\mathcal{C}_1$.

This completes the proof.

Theorem 1. *Assume $I_{m,i}(x)$ is a k-th degree polynomial defined in the cell S_i which approximates a smooth function $I(x) \geq 0$ to $(k+1)$-th order accuracy, and $I_{m,i}(x_{i+1/2}) \geq 0$, then the limited polynomial $\hat{I}_{m,i}(x)$ defined through $\check{I}_{m,i}(x)$ by the procedure above, where $\check{I}_{m,i}(x)$ is obtained by rotating the polynomial $I_{m,i}(x)$ around the point $C(\hat{x}_i^N, I_{m,i}(\hat{x}_i^N))$ clockwise by the angle $\theta_{m,i}$ described above, achieves positivity $\hat{I}_{m,i}(\hat{x}_i^\alpha) \geq 0$ for $\alpha = 1, ..., N$ and maintains the same $(k+1)$-th order accuracy for approximating $I(x)$.*

Proof: In the transformation (3.6), we take $x = \hat{x}_i^\alpha, x' = \hat{x}_i^{'\alpha}$, $x_c = \hat{x}_i^N$ and get,

$$\begin{bmatrix} \check{I}_{m,i}(\hat{x}_i^{'\alpha}) \\ \hat{x}_i^{'\alpha} \end{bmatrix} = \begin{bmatrix} \cos\theta_{m,i} & \sin\theta_{m,i} \\ -\sin\theta_{m,i} & \cos\theta_{m,i} \end{bmatrix} \begin{bmatrix} I_{m,i}(\hat{x}_i^\alpha) - I_{m,i}(\hat{x}_i^N) \\ \hat{x}_i^\alpha - \hat{x}_i^N \end{bmatrix} + \begin{bmatrix} I_{m,i}(\hat{x}_i^N) \\ \hat{x}_i^N \end{bmatrix}.$$

After a simple manipulation, the above equation can be rewritten as follows

$$\begin{array}{c} \check{I}_{m,i}(\hat{x}_i^{'\alpha}) - I(\hat{x}_i^\alpha) = \cos\theta_{m,i}(I_{m,i}(\hat{x}_i^\alpha) - I(\hat{x}_i^\alpha)) \\ +(\cos\theta_{m,i} - 1)(I(\hat{x}_i^\alpha) - I_{m,i}(\hat{x}_i^N)) + \sin\theta_{m,i}(\hat{x}_i^\alpha - \hat{x}_i^N) \end{array} , \tag{3.10}$$

$$\hat{x}_i^{'\alpha} - \hat{x}_i^\alpha = -\sin\theta_{m,i}(I_{m,i}(\hat{x}_i^\alpha) - I(\hat{x}_i^\alpha)) - \sin\theta_{m,i}(I(\hat{x}_i^\alpha) - I_{m,i}(\hat{x}_i^N)) + (\cos\theta_{m,i} - 1)(\hat{x}_i^\alpha - \hat{x}_i^N). \tag{3.11}$$

From the equality (3.11), we can obtain

$$I(\hat{x}_i^\alpha) - I_{m,i}(\hat{x}_i^N) = -\frac{1}{\sin\theta_{m,i}}(\hat{x}_i^{'\alpha} - \hat{x}_i^\alpha) - (I_{m,i}(\hat{x}_i^\alpha) - I(\hat{x}_i^\alpha)) + \frac{\cos\theta_{m,i} - 1}{\sin\theta_{m,i}}(\hat{x}_i^\alpha - \hat{x}_i^N).$$

Substituting the above expression of $I(\hat{x}_i^\alpha) - I_{m,i}(\hat{x}_i^N)$ into the equality (3.10), we obtain

$$\check{I}_{m,i}(\hat{x}_i^{'\alpha}) - I(\hat{x}_i^\alpha) = I_{m,i}(\hat{x}_i^\alpha) - I(\hat{x}_i^\alpha) + 2\tan\frac{\theta_{m,i}}{2}(\hat{x}_i^\alpha - \hat{x}_i^N) + \tan\frac{\theta_{m,i}}{2}(\hat{x}_i^{'\alpha} - \hat{x}_i^\alpha). \tag{3.12}$$

By using the result of Lemma 1, it is straightforward to prove that

$$|\check{I}_{m,i}(\hat{x}_i^{'\alpha}) - I_m(\hat{x}_i^{\alpha})| \leq \mathcal{C}h^{k+1}.$$

Since $\hat{I}_{m,i}(\hat{x}_i^{\alpha}) = \check{I}_{m,i}(\hat{x}_i^{'\alpha})$, we also have $|\hat{I}_{m,i}(\hat{x}_i^{\alpha}) - I(\hat{x}_i^{\alpha})| \leq \mathcal{C}h^{k+1}$ for all $\alpha = 1, ..., N$, which implies that $\hat{I}_{m,i}(x)$ approximates the function $I(x)$ with $(k+1)$-th order accuracy in S_i.

This completes the proof.

The easiest way to implement the rotational limiter is through the values of the limited polynomial $\hat{I}_{m,i}(x)$ at the $N = k+1$ Gauss-Lobatto points, as described above. This would involve a Lagrangian basis set (consisting of basis functions which achieve the value 1 at one Gauss-Lobatto point and 0 at other Gauss-Lobatto points). If other basis functions are used, a change of coefficients under different basis sets is needed. We emphasize that neither the DG method itself nor the rotational limiter depends on the particular choice of basis functions for the implementation.

We now summarize the limiting procedure to obtain a high order positivity-preserving scheme for solving (2.14) as follows. Here we assume that the values of radiative intensity at the boundary and the cell average of the extra source term $\bar{q}_i$ are all positive.

If $I_{m,i'}^{(\ell)}(\hat{x}_{i'}^{\alpha}) \geq 0, \forall \alpha, i', m$ and $I_{m,i'}^{(\ell+1)}(\hat{x}_{i'}^{\alpha}) \geq 0$ for all α, i', m in the upstream cells, then we have $\bar{\phi}_{m,i}^{(*)} \geq 0$ and from (3.1)-(3.2) we know at least one of $\bar{I}_{m,i}^{(\ell+1)}$ and $I_{m,i}^{(\ell+1)}(x_{i+1/2})$ is nonnegative. Then,

- If $\bar{I}_{m,i}^{(\ell+1)} \geq 0$, the scaling limiter (3.4)-(3.5) is employed to modify the DG polynomial $I_{m,i}^{(\ell+1)}(x)$ to obtain $\hat{I}_{m,i}^{(\ell+1)}(x)$;
- Otherwise, we must have $I_{m,i}^{(\ell+1)}(x_{i+1/2}) \geq 0$, then the rotational limiter algorithm is applied on $I_{m,i}^{(\ell+1)}(x)$ to obtain $\hat{I}_{m,i}^{(\ell+1)}(x)$.

Remark 1. *The procedure for the case of $\mu_m < 0$ can be obtained symmetrically.*

Remark 2. *Clearly, if the scaling limiter is used, the cell average of the DG polynomial is not changed, hence conservation is automatic. If the rotational limiter is used, the cell average is changed (in fact, the rotational limiter is used only if $\bar{I}_{m,i}^{(\ell+1)} < 0$, while the cell average after limiting is nonnegative, hence the cell average must have changed). This would appear to be a problem to conservation. However, the crucial property which helps us is that the limited polynomial $\hat{I}_{m,i}^{(\ell+1)}(x)$ and the original polynomial $I_{m,i}^{(\ell+1)}(x)$ share the same value at $x_{i+1/2}$ (or at $x_{i-1/2}$ for the $\mu_m < 0$ case). Therefore, the difference between the two Riemann sums approximating the weak formulation $-\int_{S_i} I(x)\psi_x(x)dx$ with a smooth function $\psi(x)$:*

$$D_m = \sum_i \bar{\hat{I}}_{m,i}^{(\ell+1)} \psi_x(x_i)\Delta x_i - \sum_i \bar{I}_{m,i}^{(\ell+1)} \psi_x(x_i)\Delta x_i,$$

is bounded by

$$\begin{aligned}|D_m| &= |\sum_{i\in A}(\bar{\hat{I}}_{m,i}^{(\ell+1)} - \bar{I}_{m,i}^{(\ell+1)})\psi_x(x_i)\Delta x_i| \\ &\le Ch\sum_{i\in A}|\bar{\hat{I}}_{m,i}^{(\ell+1)} - \hat{I}_{m,i}^{(\ell+1)}(x_{i+1/2}) + I_{m,i}^{(\ell+1)}(x_{i+1/2}) - \bar{I}_{m,i}^{(\ell+1)}| \\ &\le Ch\left(\sum_{i\in A}|\bar{\hat{I}}_{m,i}^{(\ell+1)} - \hat{I}_{m,i}^{(\ell+1)}(x_{i+1/2})| + \sum_{i\in A}|I_{m,i}^{(\ell+1)}(x_{i+1/2}) - \bar{I}_{m,i}^{(\ell+1)}|\right) \\ &\le Ch\left(TV(\hat{I}_{m,i}^{(\ell+1)}) + TV(I_{m,i}^{(\ell+1)})\right),\end{aligned}$$

where A is the set of cells in which the rotational limiter is applied. Therefore, this difference goes to zero when the mesh size $h \to 0$, provided both $I_{m,i}^{(\ell+1)}$ and $\hat{I}_{m,i}^{(\ell+1)}$ have bounded total variation. That is, if the numerical solution converges with bounded total variation towards a function I, then I is a weak solution of the original equation and will thus have the correct discontinuity location and strength. This is to say that our limited scheme satisfies the classical Lax-Wendroff theorem [14], which is the main purpose of using conservative schemes.

Remark 3. *We could actually also take the number of Gauss-Lobatto points $N < k+1$ as long as $2N-3 \ge k$ (this is possible when $k \ge 3$) to save cost for the limiter. Positivity can still be achieved. The order of accuracy can be maintained when we take the limited polynomial $\hat{I}_{m,i}(x)$ to interpolate $\hat{I}_{m,i}(\hat{x}_i^\alpha) = \check{I}_{m,i}(\hat{x}_i^{'\alpha}), \alpha = 1, ..., N-1$ and $\hat{I}_{m,i}(\hat{x}_i^N) = I_{m,i}(\hat{x}_i^N)$, and to be closest to the original $I_{m,i}(x)$ in the L^2-norm (least square) subject to such interpolation properties. For simplicity of presentation we do not pursue this route further in this paper.*

3.2. High order positivity-preserving DG scheme for the unsteady radiative transfer equation. The high order positivity-preserving DG scheme proposed in the previous subsection for the steady radiative transfer equation can be easily extended to the fully discrete unsteady radiative transfer equation with backward Euler time discretization. In fact, comparing equation (2.14) with equation (2.16), we find that they are the same except that σ_t, $q_{m,i}(x)$ and $I_{m,i}^{(\ell+1)}(x)$ are replaced by $\tilde{\sigma}_t$, $\tilde{q}_{m,i}(x)$ and $I_{m,i}^{n+1,(\ell+1)}(x)$, respectively. Thus the same procedure can be applied, and we do not repeat the details.

4. High order positivity-preserving DG scheme for solving the radiative transfer equation in two spatial dimensions.

4.1. The DG method for the steady radiative transfer equation in two spatial dimensions. Consider the steady radiative transfer equation in two spatial dimensions (2.2) with the domain $\mathcal{D} = [a,b] \times [c,d]$ and the rectangular mesh of $\mathcal{D} = \cup_{i=1,\cdots,N_x, j=1,\cdots,N_y} S_{i,j}$ with $S_{i,j} = [x_{i-1/2}, x_{i+1/2}] \times [y_{j-1/2}, y_{j+1/2}]$ as shown in Figure 4.1 (left). For simplicity, we only illustrate how to implement the limiter in the direction (ζ_m, η_l) with $\zeta_m > 0$ and $\eta_l > 0$, that is, its outflow boundary $\partial S_{i,j}^+ = \Gamma_{out1} \cup \Gamma_{out2}$ and inflow boundary $\partial S_{i,j}^- = \Gamma_{in1} \cup \Gamma_{in2}$ (see Figure 4.1 (left)) can be written as follows,

$$\begin{aligned}&\Gamma_{in1} = x_{i-1/2} \times [y_{j-1/2}, y_{j+1/2}], \quad \Gamma_{in2} = [x_{i-1/2}, x_{i+1/2}] \times y_{j-1/2}, \\ &\Gamma_{out1} = [x_{i-1/2}, x_{i+1/2}] \times y_{j+1/2}, \quad \Gamma_{out2} = x_{i+1/2} \times [y_{j-1/2}, y_{j+1/2}].\end{aligned}$$

The implementation for the other three cases can be obtained symmetrically.

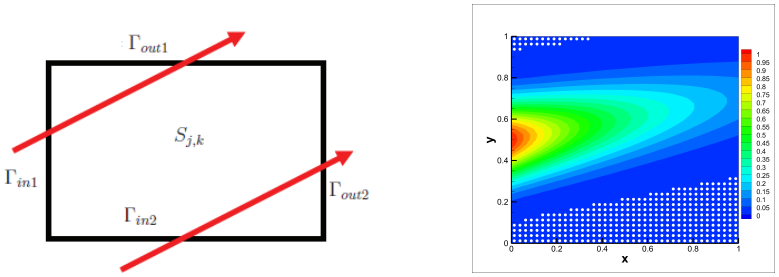

FIG. 4.1. *Left:The inflow and outflow boundaries for the direction* $\mathbf{\Omega}_{m,l} = (\zeta_m, \eta_l)$ *with* $\zeta_m > 0$ *and* $\eta_l > 0$ *in the rectangular cell* $S_{i,j}$*; Right: The radiative intensity for the purely absorbing model simulated by the* Q^1 *DG scheme with the positivity-preserving limiter on a* 40×40 *uniform grid. The white points represent the cells where the positivity-preserving limiter has been enacted during the computation.*

The DOM equation of (2.2) solved by the source iteration method can be written as

$$\zeta_m \frac{\partial I_{m,l}^{(\ell+1)}(\mathbf{r})}{\partial x} + \eta_l \frac{\partial I_{m,l}^{(\ell+1)}(\mathbf{r})}{\partial y} + \sigma_t I_{m,l}^{(\ell+1)}(\mathbf{r}) = \frac{\sigma_s}{4\pi}\phi^{(*)}(\mathbf{r}) + q(\mathbf{r}, \zeta_m, \eta_l) \tag{4.1}$$

where

$$\phi^{(*)}(\mathbf{r}) = \sum_{m',l'=1}^{M,L} \omega_{m',l'} I_{m',l'}^{(*)}(\mathbf{r}).$$

Similarly as the case in one spatial dimension, $I_{m',l'}^{(*)}(\mathbf{r})$ is taken as $I_{m',l'}^{(\ell+1)}(\mathbf{r})$ if it has already been obtained, otherwise, it is taken as $I_{m',l'}^{(\ell)}(\mathbf{r})$.

The DG method for the equation (4.1) in a rectangular cell $S_{i,j}$ can be written as

(4.2)
$$\begin{aligned}
&\int_{S_{i,j}} (-\zeta_m I_{m,l;i,j}^{(\ell+1)}(x,y)\tfrac{\partial b_{i,j}(x,y)}{\partial x} - \eta_l I_{m,l;i,j}^{(\ell+1)}(x,y)\tfrac{\partial b_{i,j}(x,y)}{\partial y} + \sigma_t I_{m,l;i,j}^{(\ell+1)}(x,y) b_{i,j}(x,y))dxdy \\
&+\eta_l \int_{\Gamma_{out1}} I_{m,l;i,j}^{(\ell+1)}(x,y) b_{i,j}(x,y)dx + \zeta_m \int_{\Gamma_{out2}} I_{m,l;i,j}^{(\ell+1)}(x,y) b_{i,j}(x,y)dy \\
&= \int_{S_{i,j}} \tfrac{\sigma_s}{4\pi}\phi_{i,j}^{(*)}(x,y) b_{i,j}(x,y)dxdy + \int_{S_{i,j}} q_{m,l}(x,y) b_{i,j}(x,y)dxdy + \\
&\zeta_m \int_{\Gamma_{in1}} I_{m,l;i-1,j}^{(\ell+1)}(x,y) b_{i,j}(x,y)dy + \eta_l \int_{\Gamma_{in2}} I_{m,l;i,j-1}^{(\ell+1)}(x,y) b_{i,j}(x,y)dx
\end{aligned}$$

where $I_{m,l;i,j}(x,y)$ is the DG solution polynomial in the cell $S_{i,j}$, and $b_{i,j}(x,y)$ is a test function. Both $I_{m,l;i,j}(x,y)$ and $b_{i,j}(x,y)$ are polynomials of degree at most k in each variable (tensor-product polynomials, denoted by Q^k).

4.2. The high order positivity-preserving DG scheme for the two-dimensional steady radiative transfer equation. Taking $b_{i,j}(x,y) = 1$, the DG method (4.2) gives

(4.3)
$$\begin{aligned}
&\sigma_t \Delta x_j \Delta y_j \tilde{\bar{I}}_{m,l;i,j}^{(\ell+1)} + \eta_l \Delta x_i \bar{I}_{m,l;i,j}^{(\ell+1)}(y_{j+1/2}) + \zeta_m \Delta y_j \tilde{I}_{m,l;i,j}^{(\ell+1)}(x_{i+1/2}) = \\
&\tfrac{\sigma_s}{4\pi}\Delta x_i \Delta y_j \tilde{\bar{\phi}}_{i,j}^{(*)} + \Delta x_i \Delta y_j \tilde{\bar{q}}_{m,l;i,j} + \zeta_m \Delta y_j \tilde{I}_{m,l;i-1,j}^{(\ell+1)}(x_{i-1/2}) + \eta_l \Delta x_i \bar{I}_{m,l;i,j-1}^{(\ell+1)}(y_{j-1/2})
\end{aligned}$$

where, for any function p, we denote

$$\begin{aligned}
&\tilde{\bar{p}}_{i,j} = \tfrac{1}{\Delta x_i \Delta y_j}\int_{x_{i-1/2}}^{x_{i+1/2}}\int_{y_{j-1/2}}^{y_{j+1/2}} p_{i,j}(x,y)dxdy, \\
&\bar{p}_{i,j'}(y_{j'+1/2}) = \tfrac{1}{\Delta x_i}\int_{x_{i-1/2}}^{x_{i+1/2}} p_{i,j'}(x, y_{j'+1/2})dx, \qquad j' = j-1, j, \\
&\tilde{p}_{i',j}(x_{i'+1/2}) = \tfrac{1}{\Delta y_j}\int_{y_{j-1/2}}^{y_{j+1/2}} p_{i',j}(x_{i'+1/2}, y)dy, \qquad i' = i-1, i.
\end{aligned}$$

That is, we use $\bar{(\cdot)}$ to denote the cell averaging operator in the x-direction, $\tilde{(\cdot)}$ to denote the cell averaging operator in the y-direction, and $\tilde{\bar{(\cdot)}}$ to denote the two dimensional cell averaging operator in the cell $S_{i,j}$.

In the cell $S_{i,j}$, by the mean value theorem, there exists $(\xi,\nu)\in S_{i,j}$ such that

(4.4)
$$I^{(\ell+1)}_{m,l;i,j}(\xi,\nu)=\frac{\sigma_t\Delta x_i\Delta y_j\tilde{\bar{I}}^{(\ell+1)}_{m,l;i,j}+\eta_l\Delta x_i\bar{I}^{(\ell+1)}_{m,l;i,j}(y_{j+1/2})+\zeta_m\Delta y_j\tilde{I}^{(\ell+1)}_{m,l;i,j}(x_{i+1/2})}{\sigma_t\Delta x_i\Delta y_j+\eta_l\Delta x_i+\zeta_m\Delta y_j}.$$

Suppose the source term $q_{m,l}(x,y)$ and $I^{(\ell+1)}_{m,l;i,j}(x,y)$ at the domain boundary are nonnegative, and the values of the DG polynomials $I^{(\ell)}_{m,l;i',j'}(x,y)$ and $I^{(\ell+1)}_{m,l;i',j'}(x,y)$ in the upstream cells (which have already been updated) at the Gauss-Lobatto points are also nonnegative (which is achieved by using the positivity-preserving limiter described below in the upstream cells), then we know that $\tilde{\bar{\phi}}^{(*)}_{i,j}$, $\tilde{\bar{q}}_{m,l;i,j}$, $\tilde{I}^{(\ell+1)}_{m,l;i-1,j}(x_{i-1/2})$, $\bar{I}^{(\ell+1)}_{m,l;i,j-1}(y_{j-1/2})$ are all nonnegative, thus we can see that $I^{(\ell+1)}_{m,l;i,j}(\xi,\nu)$ defined by (4.4) is nonnegative by (4.3), i.e., at least one term among $\tilde{\bar{I}}^{(\ell+1)}_{m,l;i,j}$, $\tilde{I}^{(\ell+1)}_{m,l;i,j}(x_{i+1/2})$ and $\bar{I}^{(\ell+1)}_{m,l;i,j}(y_{j+1/2})$ is nonnegative. Again, we emphasize that this nonnegative result is a property of the DG scheme which is valid *before* the limiter is applied in the current cell $S_{i,j}$.

We denote the Gauss-Lobatto points in the cell $S_{i,j}$ as $G_{i,j}=G_i\times G_j$, where $G_i=\{x_{i-1/2}=\hat{x}^1_i,\hat{x}^2_i,\cdots,\hat{x}^{N-1}_i,\hat{x}^N_i=x_{i+1/2}\}$, $G_j=\{y_{j-1/2}=\hat{y}^1_j,\hat{y}^2_j,\cdots,\hat{y}^{N-1}_j,\hat{y}^N_j=y_{j+1/2}\}$. For convenience, we denote the Gauss-Lobatto points in $G_{i,j}$ as $\hat{\mathbf{r}}^{\alpha_1,\alpha_2}_{i,j}=(\hat{x}^{\alpha_1}_i,\hat{y}^{\alpha_2}_j)$.

Next, in order to obtain a nonnegative solution, we will perform either the positivity-preserving scaling limiter or the positivity-preserving rotational limiter on $I_{m,l;i,j}(x,y)$, depending on which is nonnegative among $\tilde{\bar{I}}^{(\ell+1)}_{m,l;i,j}$, $\tilde{I}^{(\ell+1)}_{m,l;i,j}(x_{i+1/2})$ and $\bar{I}^{(\ell+1)}_{m,l;i,j}(y_{j+1/2})$.

4.2.1. The positivity-preserving scaling limiter in two spatial dimensions. If $\tilde{\bar{I}}_{m,l;i,j}$ is nonnegative, we will employ the scaling limiter proposed in [33], which can be described as

$$\hat{I}^{(\ell+1)}_{m,l;i,j}(x,y)=\lambda(I^{(\ell+1)}_{m,l;i,j}(x,y)-\tilde{\bar{I}}^{(\ell+1)}_{m,l;i,j})+\tilde{\bar{I}}^{(\ell+1)}_{m,l;i,j} \tag{4.5}$$

with

$$\lambda=\min\left\{\left|\frac{\tilde{\bar{I}}^{(\ell+1)}_{m,l;i,j}}{\tilde{\bar{I}}^{(\ell+1)}_{m,l;i,j}-z_{i,j}}\right|,1\right\},\qquad z_{i,j}=\min_{\hat{\mathbf{r}}^{\alpha_1,\alpha_2}_{i,j}\in G_{i,j}}(I^{(\ell+1)}_{m,l;i,j}(\hat{\mathbf{r}}^{\alpha_1,\alpha_2}_{i,j}),0). \tag{4.6}$$

Then for all $\hat{\mathbf{r}}^{\alpha_1,\alpha_2}_{i,j},\alpha_1,\alpha_2=1,..,N$, it is easy to check that $\hat{I}_{m,l;i,j}(\hat{\mathbf{r}}^{\alpha_1,\alpha_2}_{i,j})$ is nonnegative. This scaling limiter maintains the original $(k+1)$-th order accuracy, as proved in [33].

4.2.2. The positivity-preserving rotational limiter in two spatial dimensions. If $\tilde{\bar{I}}_{m,l;i,j}$ is negative, then at least one of $\tilde{I}^{(\ell+1)}_{m,l;i,j}(x_{i+1/2})$ and $\bar{I}^{(\ell+1)}_{m,l;i,j}(y_{j+1/2})$ should be nonnegative by (4.3). In this case, the limiting procedure consists of a one-dimensional scaling limiter on the relevant cell boundary followed by a two-dimensional rotational limiter around this cell boundary. For simplicity, we only illustrate how to implement the limiting procedure when $\tilde{I}^{(\ell+1)}_{m,l;i,j}(x_{i+1/2})\geq 0$.

First we modify the polynomial $I_{m,l;i,j}(x,y) \in V_h^k(S_{i,j})$ as follows. At the right boundary of the cell $x = x_{i+1/2}$, we apply the one dimensional scaling limiter to obtain

$$\check{I}^{(\ell+1)}_{m,l;i,j}(x_{i+1/2},y) = \lambda(I^{(\ell+1)}_{m,l;i,j}(x_{i+1/2},y) - \tilde{I}^{(\ell+1)}_{m,l;i,j}(x_{i+1/2})) + \tilde{I}^{(\ell+1)}_{m,l;i,j}(x_{i+1/2}) \tag{4.7}$$

where the parameter λ is determined as

$$\lambda = \min\left\{\left|\frac{\tilde{I}^{(\ell+1)}_{m,l;i,j}(x_{i+1/2})}{\tilde{I}^{(\ell+1)}_{m,l;i,j}(x_{i+1/2}) - z_{i,j}}\right|, 1\right\}, \qquad z_{i,j} = \min_{\hat{y}_j^{\alpha_2}\in G_j}(I_{m,l;i,j}(x_{i+1/2},\hat{y}_j^{\alpha_2}), 0). \tag{4.8}$$

This determines the modified polynomial $\check{I}^{(\ell+1)}_{m,l;i,j}(x,y)$ at the right boundary of the cell $x = x_{i+1/2}$, which is positive at the Gauss-Lobatto points along this cell boundary

$$\check{I}^{(\ell+1)}_{m,l;i,j}(x_{i+1/2},\hat{y}_j^{\alpha_2}) \geq 0, \qquad \alpha_2 = 1,2,\cdots,N. \tag{4.9}$$

We then take the difference of $\check{I}^{(\ell+1)}_{m,l;i,j}(x,y)$ and $I^{(\ell+1)}_{m,l;i,j}(x,y)$ at the Gauss-Lobatto points along the right boundary of the cell $x = x_{i+1/2}$:

$$d_{\alpha_2} = \check{I}^{(\ell+1)}_{m,l;i,j}(x_{i+1/2},\hat{y}_j^{\alpha_2}) - I^{(\ell+1)}_{m,l;i,j}(x_{i+1/2},\hat{y}_j^{\alpha_2}), \qquad \alpha_2 = 1,2,...,N.$$

Clearly, we have

$$d_{\alpha_2} = O(h^{k+1}), \qquad \alpha_2 = 1,2,...,N, \tag{4.10}$$

since the one-dimensional scaling limiter does not affect the order of accuracy [33]. We now modify the values of $I^{(\ell+1)}_{m,l;i,j}$ at the other Gauss-Lobatto points as

$$\check{I}^{(\ell+1)}_{m,l;i,j}(\hat{x}_i^{\alpha_1},\hat{y}_j^{\alpha_2}) = I^{(\ell+1)}_{m,l;i,j}(\hat{x}_i^{\alpha_1},\hat{y}_j^{\alpha_2}) + d_{\alpha_2}, \quad \alpha_1 = 1,...,N;\ \alpha_2 = 1,...,N. \tag{4.11}$$

Finally, the modified polynomial $\check{I}^{(\ell+1)}_{m,l;i,j}(x,y)$ is determined by the unique interpolation polynomial in Q^k satisfying (4.11). Clearly, the modified polynomial $\check{I}^{(\ell+1)}_{m,l;i,j}(x,y)$ satisfies positivity at the Gauss-Lobatto points along the right boundary of the cell $x = x_{i+1/2}$ (see (4.9)), and is $O(h^{k+1})$ close to the original polynomial $I^{(\ell+1)}_{m,l;i,j}(x,y)$ (see (4.10)).

To guarantee the positivity-preserving of the radiative intensity at all Gauss-Lobatto points $\hat{\mathbf{r}}_{i,j}^{\alpha 1,\alpha 2} \in G_{i,j}$, we need to further apply the one-dimensional rotational limiter algorithm defined in subsection 3.1.2 to $\check{I}^{(\ell+1)}_{m,l;i,j}(x,y)$, along each line $y = \hat{y}_j^{\alpha_2}$, as follows.

The two-dimensional rotational limiter algorithm:

1. Take each point $(\hat{x}_i^N, \hat{y}_j^{\alpha_2})$, for $\alpha_2 = 1,\cdots,N$, which lies on Γ_{out2}, as the rotational center, and apply the one-dimensional rotational limiter algorithm along the line $y = \hat{y}_j^{\alpha_2}$, with rotational angle $\theta^{\alpha_2}_{m,l;i,j}$, to obtain the modified values at all the Gauss-Lobatto points along this line and the modified one-dimensional polynomial $\hat{I}^{(\ell+1)}_{m,l;i,j}(x,\hat{y}_j^{\alpha_2})$. We then have

$$\hat{I}^{(\ell+1)}_{m,l;i,j}(\hat{x}_i^{\alpha_1},\hat{y}_j^{\alpha_2}) \geq 0, \qquad \alpha_1 = 1,\cdots,N.$$

2. The final limited polynomial $\hat{I}^{(\ell+1)}_{m,l;i,j}(x,y)$ is the unique interpolation polynomial in Q^k with the values at all Gauss-Lobatto points $(\hat{x}_i^{\alpha_1}, \hat{y}_j^{\alpha_2})$ with $\alpha_1 = 1, \cdots, N,\ \alpha_2 = 1, \cdots, N$, as obtained in Step 1 above.

Remark 4. *It is straightforward to prove that this limiter maintains the original high order accuracy, since we are only applying the one-dimensional rotational limiter along each line.*

The implementation of the positivity-preserving limiter is simple. Specifically the flowchart for the 2D positivity-preserving limiter is as follows. Again, we list the algorithm flowchart only for the case of $\zeta_m > 0, \eta_l > 0$, as the other three cases can be obtained symmetrically.

1. If $\tilde{\bar{I}}_{m,l;i,j} \geq 0$ then
   perform the scaling limiter (4.5)-(4.6) on $I_{m,l;i,j}(x,y)$ to obtain $\hat{I}_{m,l;i,j}(x,y)$;
2. else if $\tilde{I}_{m,l;i,j}(x_{i+1/2}) \geq 0$ then
   perform (4.7)-(4.8) and (4.11) on $I_{m,l;i,j}(x,y)$ to obtain $\check{I}_{m,l;i,j}(x,y)$ first, and then perform the two-dimensional rotational limiter algorithm to obtain $\hat{I}_{m,l;i,j}(x,y)$;
3. else if $\bar{I}_{m,l;i,j}(y_{j+1/2}) \geq 0$ then
   perform the similar procedure as the second case above with the role of x and y switched to obtain $\hat{I}_{m,l;i,j}(x,y)$.

Finally the polynomial $\hat{I}^{(\ell+1)}_{m,l;i,j}(x,y)$ is nonnegative at all Gauss-Lobatto points in the cell $S_{i,j}$ and hence the cell-average of $\hat{I}_{m,l;i,j}(x,y)$ is also nonnegative. The original high order accuracy is maintained.

Remark 5. *Similarly as for the one-dimensional high order positivity-preserving DG scheme, the two-dimensional high order positivity-preserving DG scheme proposed for the steady radiative transfer equation can also be easily extended to the unsteady radiative transfer equation. We do not repeat the details here.*

5. Numerical results. In this section, we perform numerical experiments in one- and two-dimensions to validate the properties of high order accuracy and positivity-preserving of our DG schemes. Regarding the discrete-ordinate quadrature rule, we adopt the Legendre-Chebyshev P_N-T_N quadrature [13] in which the μ-levels are equal to the roots of the Gauss-Legendre quadrature, and the azimuthal angles are determined from the roots of the orthogonal Chebyshev (T_N) polynomials. To be more specific, S_8 and P_8-T_8 are used for all the following one-dimensional and the two-dimensional tests with non-zero scattering terms respectively, unless otherwise stated. The figures and tables involved in the DG scheme with the positivity preserving limiter are given by the limiting procedures described in the previous sections, unless otherwise stated.

Example 1. *(The accuracy test of the DG schemes for the one-dimensional steady radiative transfer equation)*

In this test, we solve the absorbing-scattering radiative transfer problem described by the equation (2.3) with $\sigma_t = 22000$, $\sigma_s = 1$, $q(x,\mu) = -4\pi\mu^3 \cos^3 \pi x \sin \pi x + \sigma_t(\mu^2 \cos^4 \pi x + a) - \sigma_s(a + \frac{\cos^4 \pi x}{3})$. *Here* $a = 10^{-14}$ *is a small positive constant which is used to ensure the source term to be nonnegative. The computational domain is* $\mathcal{D} = [0,1]$. *The boundary condition is given as follows*

$$\begin{cases} I(0,\mu) = \mu^2 + a, & if\ \ \mu > 0, \\ I(1,\mu) = \mu^2 + a, & if\ \ \mu < 0. \end{cases}$$

For this problem, we have the exact solution given as $I(x,\mu) = \mu^2 \cos^4 \pi x + a$.

We perform the test on the DG scheme without and with the positivity-preserving limiter respectively. For the DG scheme with the positivity-preserving limiter, we test the following two types: 1) Judge if $\bar{I}_{m,i}^{(\ell+1)} \geq 0$ first. If yes, then the scaling limiter is employed; if not, then the rotational limiter is applied. This is the algorithm that we presented in the previous sections and we name it as "scaling limiter preferred". It should be used in practical computations since it has smaller conservation error by preferring the scaling limiter which does not change cell averages; 2) Judge if $I_{m,i}^{(\ell+1)}(x_{i+1/2}) \geq 0$ first. If yes, then the rotational limiter is applied; if not, then the scaling limiter is used. We name this procedure as "rotational limiter preferred". This option is tested simply to see how much conservation error will incur when the rotational limiter is applied to the maximum extent. In order to estimate the conservation error incurred by the implementation of the rotational limiter, we define it by $\frac{1}{(b-a)M}\sum_{m,i}(\bar{\hat{I}}_{m,i} - \bar{I}_{m,i})\Delta x_i$ in the final iteration step, where $\bar{I}_{m,i}$ and $\bar{\hat{I}}_{m,i}$ are the cell averages of the polynomials for the cell S_i in the m-th direction before and after the positivity-preserving limiter is employed respectively.

The left two figures in Fig. 5.1 show the comparison of I simulated by the P^1 DG scheme without and with the positivity-preserving limiter (type 1 above) using 40 uniform cells. From the figures, we can observe that negative values do occur in the solution of the P^1 DG scheme without the positivity-preserving limiter, while the P^1 DG scheme with the positivity-preserving limiter produces nonnegative results. The errors and orders of accuracy for the $\{P^1, P^2, P^3, P^4\}$ DG schemes without the positivity-preserving limiter and with the positivity-preserving limiter (both rotational limiter preferred and scaling limiter preferred procedures) are shown in Tables 5.1-5.4 respectively. In these tables, we also list the percentage of the cells where the rotational positivity-preserving limiter (denoted as "rot" in the tables) and either type of positivity-preserving limiters (denoted as "tol" in the tables) are enacted during the computation respectively. The conservation errors (denoted as "*c_err* " in the tables) produced by the positivity-preserving limiters are also shown in the tables. We can clearly see from these tables that the DG schemes with the above mentioned two types of the positivity-preserving limiting procedures can achieve the same designed order of accuracy as the DG schemes without the positivity-preserving limiter both in the L_2 and L_∞ norms, while the DG schemes with the positivity-preserving limiter can also keep the positivity of the radiative intensity. We also notice that the scaling limiter does not incur any conservation error as expected, while the conservation error produced by the rotational limiter converges to 0 asymptotically with the refinement of the grid, and higher order DG schemes generate smaller conservation errors. We also notice that, for the type 1 limiting procedure preferring the scaling limiter, the rotational limiter is never enacted in this test case, indicating that the cell averages stay non-negative for the unlimited DG solution.

Example 2. *(The accuracy test of the DG schemes for the one-dimensional unsteady radiative transfer equation)*

To simulate the one-dimensional unsteady transfer equation (2.9), the same domain and parameters σ_t, σ_s and a are taken as those in the previous example. The source term is given as $q(x,\mu,t) = -4\pi\mu^2\cos^3\pi(x+t)\sin\pi(x+t)(\frac{1}{c}+\mu)+\sigma_t(\mu^2\cos^4\pi(x+t)+a) - \sigma_s(a+\frac{\cos^4\pi(x+t)}{3})$. $c = 3.0\times 10^8$. *The initial condition is* $I(x,\mu,0) = \mu^2\cos^4\pi x + a$. *The boundary conditions are given as*

$$\begin{cases} I(0,\mu,t) = \mu^2\cos^4\pi t + a, & if\ \ \mu > 0, \\ I(1,\mu,t) = \mu^2\cos^4\pi(1+t) + a, & if\ \ \mu < 0. \end{cases}$$

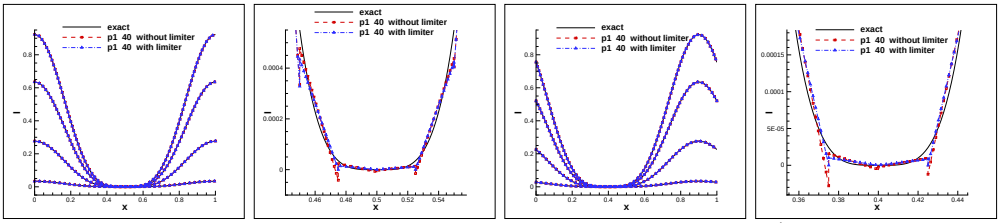

FIG. 5.1. *The comparison of the radiative intensity simulated by the P^1 DG scheme without and with the (type 1) positivity-preserving limiter on a 40 uniform grid. The left two figures are the radiative intensity for the 1D steady radiative transfer equation in the whole domain and directions and in the zoomed region at the direction $\mu = -0.9603$ respectively; The right two figures are the radiative intensity for the 1D unsteady radiative transfer equation in the whole domain and directions and in the zoomed region at the direction $\mu = -0.7967$ respectively.*

TABLE 5.1
Errors of the P^1 DG scheme for the 1D steady radiative transfer equation

without positivity-preserving limiter							
N_x	L_2 error	L_2 order	L_∞ error	L_∞ order	rot(%)	tol(%)	c_err
10	0.293E-02		0.275E-01		-	-	-
20	0.740E-03	1.98	0.741E-02	1.89	-	-	-
40	0.186E-03	2.00	0.189E-02	1.97	-	-	-
80	0.464E-04	2.00	0.482E-03	1.97	-	-	-
with positivity-preserving limiter (rotational limiter preferred)							
10	0.296E-02		0.275E-01		20.0	40.0	0.143E-03
20	0.741E-03	2.00	0.741E-02	1.89	10.0	20.0	0.743E-05
40	0.186E-03	2.00	0.189E-02	1.97	5.0	10.0	0.260E-06
80	0.464E-04	2.00	0.483E-03	1.97	2.5	5.0	0.842E-08
with positivity-preserving limiter (scaling limiter preferred)							
10	0.297E-02		0.275E-01		0.0	40.0	0.0
20	0.741E-03	2.00	0.741E-02	1.89	0.0	20.0	0.0
40	0.186E-03	2.00	0.189E-02	1.97	0.0	10.0	0.0
80	0.464E-04	2.00	0.482E-03	1.97	0.0	5.0	0.0

The exact solution for this model is $I(x, \mu, t) = \mu^2 \cos^4 \pi(x + t) + a$.

The final computational time is $t = 0.1$. Since our DG schemes are designed implicitly, there is no limitation on the time step for the stability requirement. But as the time derivatives are discretized by the Euler backward time stepping in our DG schemes, the schemes are high order accurate in space and but only first order accurate in time. In order to verify the spatial accuracy of the DG schemes with our limiter, we choose a small time step $\Delta t = 10^{-3}$ in order to make the spatial error dominate. For this problem, the DG schemes without the positivity-preserving limiter do produce negative results. The right two figures in Fig. 5.1 show the comparison of I simulated by the P^1 DG scheme without and with the (type 1) positivity-preserving limiter using 40 uniform cells. The errors and orders of accuracy for the $\{P^1, P^2, P^3, P^4\}$ DG schemes without and with the positivity-preserving limiter are shown in Tables 5.5-5.8 respectively. The conservation error and the percentage of the cells where the rotational positivity-preserving limiter and either of the two types of positivity-preserving limiting procedures are performed during the computation are also listed in the tables respectively. Since the performance of the algorithm "scaling limiter preferred" in this example is much similar to that in the previous example, we don't show their results

TABLE 5.2
Errors of the P^2 DG scheme for the 1D steady radiative transfer equation

without positivity-preserving limiter							
N_x	L_2 error	L_2 order	L_∞ error	L_∞ order	rot(%)	tol(%)	*c_err*
10	0.259E-03		0.255E-02		-	-	-
20	0.328E-04	2.98	0.321E-03	2.99	-	-	-
40	0.411E-05	3.00	0.403E-04	2.99	-	-	-
80	0.513E-06	3.00	0.498E-05	3.02	-	-	-
with positivity-preserving limiter (rotational limiter preferred)							
10	0.259E-03		0.255E-02		0.0	0.0	0.0
20	0.328E-04	2.98	0.321E-03	2.99	0.0	0.0	0.0
40	0.411E-05	3.00	0.403E-04	2.99	0.0	0.0	0.0
80	0.513E-06	3.00	0.498E-05	3.02	0.0	0.0	0.0
with positivity-preserving limiter (scaling limiter preferred)							
10	0.259E-03		0.255E-02		0.0	0.0	0.0
20	0.328E-04	2.98	0.321E-03	2.99	0.0	0.0	0.0
40	0.411E-05	3.00	0.403E-04	2.99	0.0	0.0	0.0
80	0.513E-06	3.00	0.498E-05	3.02	0.0	0.0	0.0

TABLE 5.3
Errors of the P^3 DG scheme for the 1D steady radiative transfer equation

without positivity-preserving limiter							
N_x	L_2 error	L_2 order	L_∞ error	L_∞ order	rot(%)	tol(%)	*c_err*
10	0.201E-04		0.184E-03		-	-	-
20	0.128E-05	3.98	0.129E-04	3.83	-	-	-
40	0.800E-07	3.99	0.850E-06	3.93	-	-	-
80	0.501E-08	4.00	0.553E-07	3.94	-	-	-
with positivity-preserving limiter (rotational limiter preferred)							
10	0.277E-04		0.455E-03		10.0	20.0	0.257E-05
20	0.162E-05	4.09	0.348E-04	3.71	5.0	10.0	0.963E-07
40	0.922E-07	4.14	0.226E-05	3.95	2.5	5.0	0.315E-08
80	0.540E-08	4.10	0.140E-06	4.01	1.3	2.5	0.100E-09
with positivity-preserving limiter (scaling limiter preferred)							
10	0.323E-04		0.457E-03		0.0	20.0	0.0
20	0.185E-05	4.13	0.351E-04	3.70	0.0	10.0	0.0
40	0.101E-06	4.20	0.230E-05	3.93	0.0	5.0	0.0
80	0.570E-08	4.15	0.146E-06	3.98	0.0	2.5	0.0

here to save space. We observe that the order of accuracy is maintained for the DG schemes after the application of the positivity-preserving limiter, as expected. The conservation error and the percentage of the limited cells of DG schemes for the 1D unsteady radiative transfer equation have a similar convergent behavior as that in DG schemes for 1D steady radiative transfer equation shown in the last example.

Example 3. *(The accuracy test of the DG schemes for the two-dimensional steady radiative transfer equation simulating the purely absorbing model)*

In this test, we solve the two-dimensional steady radiative transfer equation (2.2) with $\sigma_t = 1, \sigma_s = 0$, $q = 0$. The computational domain is $[0,1]\times[0,1]$. $\zeta = 0.5, \eta = 0.1$.

TABLE 5.4
Errors of the P^4 DG scheme for the 1D steady radiative transfer equation

without positivity-preserving limiter							
N_x	L_2 error	L_2 order	L_∞ error	L_∞ order	rot(%)	tol(%)	*c_err*
10	0.133E-05		0.125E-04		-	-	-
20	0.418E-07	4.99	0.399E-06	4.97	-	-	-
40	0.130E-08	5.01	0.122E-07	5.03	-	-	-
80	0.403E-10	5.02	0.373E-09	5.03	-	-	-
with positivity-preserving limiter (rotational limiter preferred)							
10	0.169E-05		0.181E-04		10.0	20.0	0.150E-06
20	0.436E-07	5.28	0.399E-06	5.51	5.0	10.0	0.125E-08
40	0.131E-08	5.06	0.122E-07	5.03	2.5	5.0	0.993E-11
80	0.402E-10	5.02	0.371E-09	5.04	1.3	2.5	0.785E-13
with positivity-preserving limiter (scaling limiter preferred)							
10	0.191E-05		0.183E-04		0.0	20.0	0.0
20	0.449E-07	5.41	0.399E-06	5.52	0.0	10.0	0.0
40	0.132E-08	5.09	0.122E-07	5.03	0.0	5.0	0.0
80	0.403E-10	5.03	0.373E-09	5.03	0.0	2.5	0.0

TABLE 5.5
Errors of the P^1 DG scheme for the 1D unsteady radiative transfer equation

without positivity-preserving limiter							
N_x	L_2 error	L_2 order	L_∞ error	L_∞ order	rot(%)	tol(%)	*c_err*
10	0.293E-02		0.275E-01		-	-	-
20	0.740E-03	1.98	0.744E-02	1.89	-	-	-
40	0.186E-03	2.00	0.190E-02	1.97	-	-	-
80	0.464E-04	2.00	0.483E-03	1.98	-	-	-
with positivity-preserving limiter (rotational limiter preferred)							
10	0.295E-02		0.275E-01		20.0	40.0	0.713E-04
20	0.741E-03	1.99	0.744E-02	1.89	10.0	20.0	0.372E-05
40	0.186E-03	2.00	0.190E-02	1.97	5.0	10.0	0.130E-06
80	0.464E-04	2.00	0.483E-03	1.98	2.5	5.0	0.420E-08

The boundary condition is

$$I(x,0) = 0, \qquad I(0,y) = \sin^6(\pi y).$$

In this case, the problem has the exact solution given as follows,

$$I(x,y) = \begin{cases} 0, & y < \frac{\eta}{\zeta}x, \\ \sin^6(\pi(y - \frac{\eta}{\zeta}x))e^{-\frac{\sigma_t}{\zeta}x}, & else. \end{cases} \tag{5.1}$$

For this problem, numerically negative radiative intensity appears if the positivity-preserving limiter is not used in the high order DG schemes. Figure 4.1 (right) shows the contours of the radiative intensity simulated by the Q^1 DG scheme using 40×40 uniform cells and the cells where the positivity-preserving limiter has been enacted during the simulation. The errors and orders of accuracy for the $\{Q^1, Q^2, Q^3, Q^4\}$ DG schemes without and with the positivity-preserving limiter are listed in Tables 5.9-5.12 respectively. The conservation error and the percentage of the cells that require

TABLE 5.6
Errors of the P^2 DG scheme for the 1D unsteady radiative transfer equation

without positivity-preserving limiter							
N_x	L_2 error	L_2 order	L_∞ error	L_∞ order	rot(%)	tol(%)	*c_err*
10	0.259E-03		0.256E-02		-	-	-
20	0.328E-04	2.98	0.321E-03	2.99	-	-	-
40	0.411E-05	3.00	0.403E-04	2.99	-	-	-
80	0.513E-06	3.00	0.498E-05	3.02	-	-	-
with positivity-preserving limiter (rotational limiter preferred)							
10	0.259E-03		0.256E-02		0.0	0.0	0.0
20	0.328E-04	2.98	0.321E-03	2.99	0.0	0.0	0.0
40	0.411E-05	3.00	0.403E-04	2.99	0.0	0.0	0.0
80	0.513E-06	3.00	0.498E-05	3.02	0.0	0.0	0.0

TABLE 5.7
Errors of the P^3 DG scheme for the 1D unsteady radiative transfer equation

without positivity-preserving limiter							
N_x	L_2 error	L_2 order	L_∞ error	L_∞ order	rot(%)	tol(%)	*c_err*
10	0.202E-04		0.185E-03		-	-	-
20	0.128E-05	3.98	0.131E-04	3.82	-	-	-
40	0.800E-07	3.99	0.855E-06	3.94	-	-	-
80	0.501E-08	4.00	0.555E-07	3.95	-	-	-
with positivity-preserving limiter (rotational limiter preferred)							
10	0.273E-04		0.455E-03		10.0	20.0	0.128E-05
20	0.161E-05	4.09	0.348E-04	3.71	5.0	10.0	0.481E-07
40	0.916E-07	4.13	0.226E-05	3.94	2.5	5.0	0.157E-08
80	0.537E-08	4.09	0.140E-06	4.01	1.3	2.5	0.500E-10

the usage of the two types of positivity-preserving limiters are listed in these tables as well. From these tables, we can see that the expected order of accuracy for the positivity-preserving DG schemes has been achieved, both in L_2-norm and L_∞-norm, as expected from our theoretical results. Also we can notice that the conservation error goes to 0 with grid refinement and higher order schemes incur smaller conservation errors.

Example 4. *(The positivity-preserving test of the DG schemes for the two-dimensional steady radiative transfer equation simulating the transparent model)*

This problem is a two-dimensional unity square enclosure with a transparent medium which is described by the equation (2.2) with $\sigma_t = 0, \sigma_s = 0$, $q = 0$. $\zeta = 0.7, \eta = 0.7$. The computational domain is $[0,1] \times [0,1]$. A 40×40 uniform grid is used in the computation. The boundary condition is

$$I(x,0) = 0, \qquad I(0,y) = 1.$$

For this problem, it has the exact solution given as follows,

$$I(x,y) = \begin{cases} 0, & y < \frac{\eta}{\zeta} x, \\ 1, & else. \end{cases} \tag{5.2}$$

In this test, negative solution will appear if we do not adopt the positivity-preserving limiter in the DG schemes with higher than first order, while the DG schemes with

TABLE 5.8
Errors of the P^4 DG scheme for the 1D unsteady radiative transfer equation

without positivity-preserving limiter							
N_x	L_2 error	L_2 order	L_∞ error	L_∞ order	rot(%)	tol(%)	*c_err*
10	0.133E-05		0.126E-04		-	-	-
20	0.418E-07	4.99	0.406E-06	4.95	-	-	-
40	0.130E-08	5.01	0.125E-07	5.02	-	-	-
80	0.403E-10	5.02	0.388E-09	5.01	-	-	-
with positivity-preserving limiter (rotational limiter preferred)							
10	0.167E-05		0.181E-04		10.0	20.0	0.753E-07
20	0.435E-07	5.26	0.406E-06	5.48	5.0	10.0	0.623E-09
40	0.131E-08	5.05	0.125E-07	5.02	2.5	5.0	0.496E-11
80	0.403E-10	5.02	0.388E-09	5.01	1.3	2.5	0.392E-13

TABLE 5.9
Errors of the Q^1 DG scheme for the 2D steady radiative transfer equation simulating the purely absorbing model

without positivity-preserving limiter							
$N_x = N_y$	L_2 error	L_2 order	L_∞ error	L_∞ order	rot(%)	tol(%)	*c_err*
10	0.431E-03		0.835E-01		-	-	-
20	0.118E-03	1.86	0.245E-01	1.77	-	-	-
40	0.311E-04	1.93	0.673E-02	1.87	-	-	-
80	0.795E-05	1.97	0.179E-02	1.91	-	-	-
with positivity-preserving limiter (rotational limiter preferred)							
10	0.465E-03		0.833E-01		50.0	50.0	0.249E-04
20	0.120E-03	1.96	0.245E-01	1.76	32.3	32.3	0.274E-06
40	0.311E-04	1.95	0.673E-02	1.87	21.8	21.8	0.152E-08
80	0.795E-05	1.97	0.179E-02	1.91	16.3	16.3	0.674E-11
with positivity-preserving limiter (scaling limiter preferred)							
10	0.453E-03		0.833E-01		0.0	48.0	0.0
20	0.119E-03	1.93	0.245E-01	1.76	0.0	31.5	0.0
40	0.311E-04	1.94	0.673E-02	1.87	0.0	21.1	0.0
80	0.795E-05	1.97	0.179E-02	1.91	0.0	15.8	0.0

the positivity-preserving limiter can always maintain the nonnegative solution. Figure 5.2 plots the contours of the radiative intensity simulated by the $\{Q^1, Q^2, Q^3, Q^4\}$ DG schemes with the (type 1) positivity-preserving limiter respectively. In the pictures, we mark the cells where the positivity-preserving has been enacted by discrete white points as well. Figures 5.3-5.4 show the comparison of the radiative intensity cut along the line $y = 0.5$ and $x = 0.5$ simulated by the DG schemes without and with the positivity-preserving limiter respectively. We can clearly see that the DG schemes without the positivity-preserving limiter produce negative solutions while the positivity of the radiative intensity can be kept well for the DG schemes with the positivity-preserving limiter. Also, higher order DG schemes produce more accurate solutions than the lower order DG schemes.

Example 5. *(The positivity-preserving test of the DG schemes for the two-dimensional steady radiative transfer equation simulating the purely absorbing model)*

We test the schemes on the purely absorbing model which is expressed by the

TABLE 5.10
Errors of the Q^2 DG scheme for the 2D steady radiative transfer equation simulating the purely absorbing model

without positivity-preserving limiter							
$N_x = N_y$	L_2 error	L_2 order	L_∞ error	L_∞ order	rot(%)	tol(%)	*c_err*
10	0.521E-04		0.110E-01		-	-	-
20	0.584E-05	3.16	0.154E-02	2.84	-	-	-
40	0.700E-06	3.06	0.198E-03	2.96	-	-	-
80	0.863E-07	3.02	0.251E-04	2.98	-	-	-
with positivity-preserving limiter (rotational limiter preferred)							
10	0.520E-04		0.110E-01		12.0	12.0	0.145E-05
20	0.584E-05	3.15	0.154E-02	2.84	7.8	7.8	0.122E-07
40	0.700E-06	3.06	0.198E-03	2.96	6.9	6.9	0.101E-09
80	0.863E-07	3.02	0.251E-04	2.98	6.3	6.3	0.593E-12
with positivity-preserving limiter (scaling limiter preferred)							
10	0.519E-04		0.110E-01		0.0	11.0	0.0
20	0.584E-05	3.15	0.154E-02	2.84	0.0	7.5	0.0
40	0.700E-06	3.06	0.198E-03	2.96	0.0	5.9	0.0
80	0.863E-07	3.02	0.251E-04	2.98	0.0	5.3	0.0

TABLE 5.11
Errors of the Q^3 DG scheme for the 2D steady radiative transfer equation simulating the purely absorbing model

without positivity-preserving limiter							
$N_x = N_y$	L_2 error	L_2 order	L_∞ error	L_∞ order	rot(%)	tol(%)	*c_err*
10	0.819E-05		0.234E-02		-	-	-
20	0.551E-06	3.89	0.171E-03	3.78	-	-	-
40	0.335E-07	4.04	0.111E-04	3.94	-	-	-
80	0.198E-08	4.08	0.706E-06	3.98	-	-	-
with positivity-preserving limiter (rotational limiter preferred)							
10	0.911E-05		0.234E-02		25.0	25.0	0.108E-05
20	0.562E-06	4.02	0.171E-03	3.78	17.8	17.8	0.116E-07
40	0.336E-07	4.06	0.111E-04	3.94	13.4	13.4	0.705E-10
80	0.198E-08	4.08	0.706E-06	3.98	10.6	10.6	0.371E-12
with positivity-preserving limiter (scaling limiter preferred)							
10	0.904E-05		0.234E-02		0.0	22.0	0.0
20	0.567E-06	4.00	0.171E-03	3.78	0.0	14.0	0.0
40	0.336E-07	4.08	0.111E-04	3.94	0.0	9.2	0.0
80	0.198E-08	4.08	0.706E-06	3.98	0.0	7.5	0.0

equation (2.2) with $\sigma_t = 1, \sigma_s = 0$ and $q = 0$. The computational domain is $[0,1] \times [0,1]$. $\zeta = 0.7, \eta = 0.7$. The boundary condition is

$$I(x,0) = 0, \qquad I(0,y) = 1.$$

The exact solution for this example can be described as follows,

$$I(x,y) = \begin{cases} 0, & y < \frac{\eta}{\zeta}x, \\ e^{-\frac{\sigma_t}{\zeta}x}, & else. \end{cases} \tag{5.3}$$

TABLE 5.12
Errors of the Q^4 DG scheme for the 2D steady radiative transfer equation simulating the purely absorbing model

$N_x = N_y$	L_2 error	L_2 order	L_∞ error	L_∞ order	rot (%)	tol(%)	*c_err*
without positivity-preserving limiter							
10	0.929E-06		0.274E-03		-	-	-
20	0.210E-07	5.47	0.103E-04	4.74	-	-	-
40	0.541E-09	5.28	0.335E-06	4.94	-	-	-
80	0.151E-10	5.17	0.105E-07	4.99	-	-	-
with positivity-preserving limiter (rotational limiter preferred)							
10	0.942E-06		0.274E-03		13.0	13.0	0.118E-07
20	0.210E-07	5.48	0.103E-04	4.74	11.0	11.0	0.258E-09
40	0.541E-09	5.28	0.335E-06	4.94	9.8	9.8	0.297E-11
80	0.151E-10	5.17	0.105E-07	4.99	8.5	8.5	0.184E-13
with positivity-preserving limiter (scaling limiter preferred)							
10	0.947E-06		0.274E-03		0.0	12.0	0.0
20	0.210E-07	5.49	0.103E-04	4.74	0.0	7.0	0.0
40	0.541E-09	5.28	0.335E-06	4.94	0.0	6.3	0.0
80	0.151E-10	5.17	0.105E-07	4.99	0.0	6.3	0.0

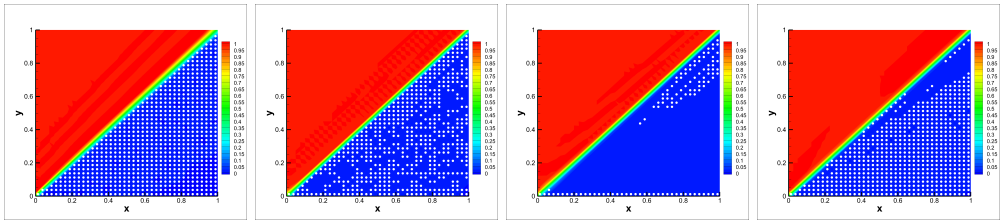

FIG. 5.2. *The contours of the radiative intensity for the transparent model simulating by the DG schemes with the positivity-preserving limiter on a 40×40 uniform grid. From left to right, 1st: Q^1; 2nd: Q^2; 3rd: Q^3; 4th: Q^4. The white points represent the cells where the positivity-preserving limiter has been enacted during the computation.*

Figures 5.5-5.7 show the results of $\{Q^1, Q^2, Q^3, Q^4\}$ DG schemes on a 40×40 uniform grid individually. To be more specific, Figure 5.5 depicts the contours of the radiative intensity simulated by the $\{Q^1, Q^2, Q^3, Q^4\}$ DG schemes with the (type 1) positivity-preserving limiter respectively, where the cells in which the positivity-preserving limiter has been enacted during the computation are marked by the discrete white points. In Figures 5.6-5.7, the comparison of the radiative intensity cut along the lines $y = 0.5$ and $x = 0.5$ obtained by the DG schemes without and with the positivity-preserving limiter is presented respectively. From these figures, we can observe that the positivity-preserving limiter is necessary for the DG schemes to produce positive solutions and the limiter can also maintain the good resolution of the DG schemes.

Example 6. *(The positivity-preserving test of the DG schemes for the two-dimensional steady radiative transfer equation simulating the absorbing-scattering model)*

In this problem, we test the schemes on the absorbing-scattering model described by the equation (2.2) with $\sigma_t = 1, \sigma_s = 1$ and $q = 0$. The computational domain is $[0, 1] \times [0, 1]$. The boundary condition is set as follows,

$$I(x, 0) = 0, \eta > 0; \qquad I(x, 1) = 0, \eta < 0;$$
$$I(0, y) = 1 - \cos(4\pi y), \zeta > 0; \qquad I(1, y) = 0, \zeta < 0.$$

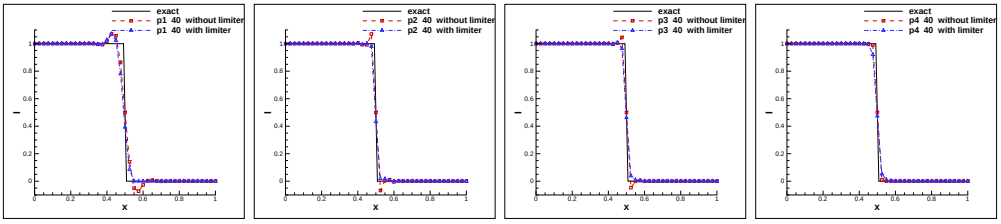

FIG. 5.3. *The comparison of the radiative intensity cut along the line $y = 0.5$ for the transparent model simulated by the DG schemes without and with the positivity-preserving limiter on a 40×40 uniform grid. From left to right, 1st: Q^1; 2nd: Q^2; 3rd: Q^3; 4th: Q^4.*

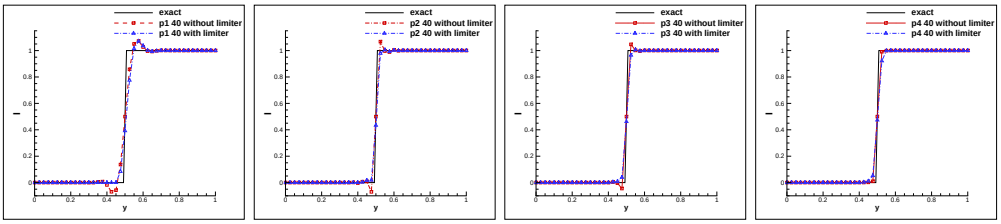

FIG. 5.4. *The comparison of the radiative intensity cut along the line $x = 0.5$ for the transparent model simulated by the DG schemes without and with the positivity-preserving limiter on a 40×40 uniform grid. From left to right, 1st: Q^1; 2nd: Q^2; 3rd: Q^3; 4th: Q^4.*

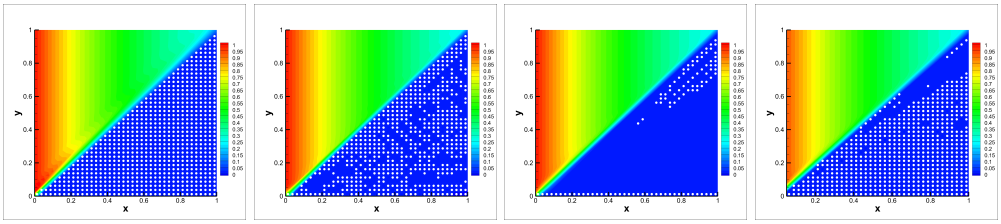

FIG. 5.5. *The contours of the radiative intensity for the purely absorbing model simulated by the DG schemes with the positivity-preserving limiter on a 40×40 uniform grid. From left to right, 1st: Q^1; 2nd: Q^2; 3rd: Q^3; 4th: Q^4. The white points represent the cells where the positivity-preserving limiter has been enacted during the computation.*

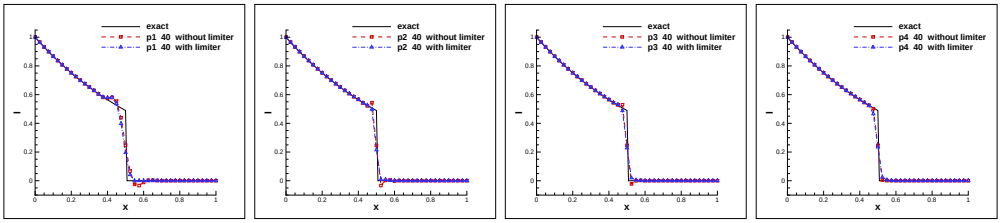

FIG. 5.6. *The comparison of the radiative intensity cut along the line $y = 0.5$ for the purely absorbing model simulated by the DG schemes without and with the positivity-preserving limiter on a 40×40 uniform grid. From left to right, 1st: Q^1; 2nd: Q^2; 3rd: Q^3; 4th: Q^4.*

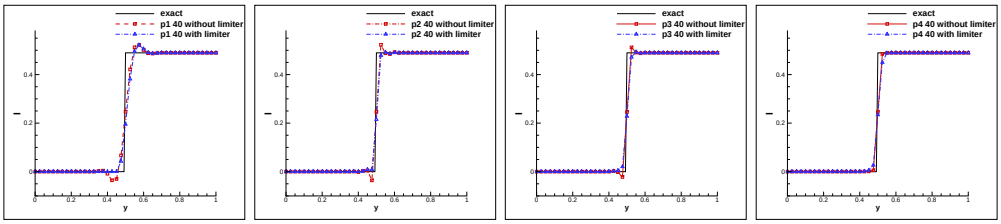

FIG. 5.7. *The comparison of the radiative intensity cut along the line $x = 0.5$ for the purely absorbing model simulated by the DG schemes without and with the positivity-preserving limiter on a 40×40 uniform grid. From left to right, 1st: Q^1; 2nd: Q^2; 3rd: Q^3; 4th: Q^4.*

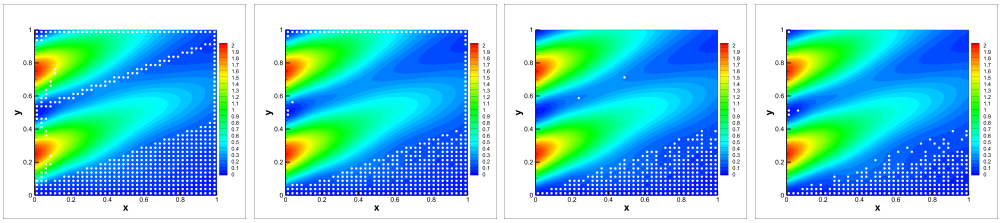

FIG. 5.8. *The contours of the radiative intensity for the absorbing-scattering model in the* $(\zeta, \eta) = (0.2578, 0.1068)$ *angular direction simulated by the DG schemes with the positivity-preserving limiter on a* 40×40 *uniform grid. From left to right, 1st:* Q^1*; 2nd:* Q^2*; 3rd:* Q^3*; 4th:* Q^4*. The white points represent the cells where the positivity-preserving limiter has been enacted during the computation.*

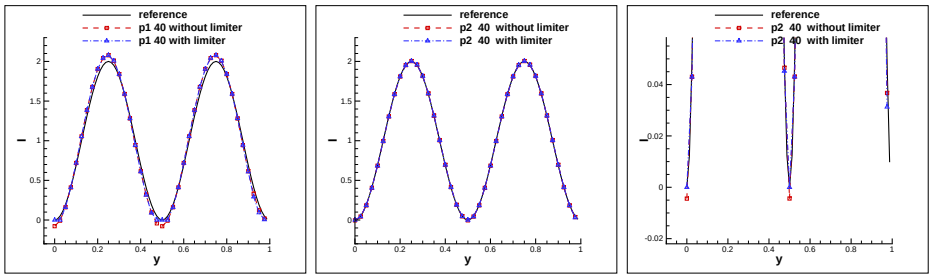

FIG. 5.9. *The comparison of the radiative intensity cut along the cells near the left boundary in the* $(\zeta, \eta) = (0.3256, -0.7860)$ *angular direction for the absorbing-scattering model simulated by the DG schemes without and with the positivity-preserving limiter. Left:* Q^1*; Middle:* Q^2*; Right: the zoomed region by* Q^2*.*

The exact solution for this problem cannot be obtained explicitly. For the purpose of comparison, we take the numerical solution by the Q^4 DG schemes with the (type 1) positivity-preserving limiter on a 80×80 uniform grid as a reference solution. We implement the test on a 40×40 uniform grid by using the different order DG schemes without and with the (type 1) positivity-preserving limiter. The contours of the radiative intensity in the $(\zeta, \eta) = (0.2578, 0.1068)$ angular direction simulated by the $\{Q^1, Q^2, Q^3, Q^4\}$ DG schemes with the positivity-preserving limiter are given in Figure 5.8. In the pictures, the cells where the positivity-preserving limiter has taken effect during the computation are marked by discrete white points as well. Figure 5.9 shows the comparison of the radiative intensity cut along the cells near the left boundary in the $(\zeta, \eta) = (0.3256, -0.7860)$ angular direction simulated by the $\{Q^1, Q^2\}$ DG schemes without and with the positivity-preserving limiter individually. From these figures, we notice that negative solution will appear if the high order DG schemes without the positivity-preserving limiter are used, while the high order DG schemes with the positivity-preserving limiter can produce nonnegative solutions with good resolution.

6. Concluding remarks. In this paper, we present a methodology to construct positivity-preserving discontinuous Galerkin (DG) schemes in one- and two-dimensional spaces for steady and unsteady radiative transfer equations. We develop a positivity-preserving limiter, which is a combination of the (now well known) scaling limiter in [33] and a new rotational limiter. It can be proved that this limiter keeps the radiative intensity nonnegative and also maintains convergence to weak solutions with the originally designed high order accuracy in smooth regions. The numerical results of steady and unsteady radiative transfer problems demonstrate the

effectiveness of our high order positivity-preserving DG schemes. Although in this paper we only discuss the scheme on rectangular meshes up to two spatial dimensions using tensor product polynomials, the idea can be extended to arbitrary meshes with P^k polynomials and to higher dimensions, which constitutes our future work. The generalization of the positivity-preserving DG schemes to other coordinates such as cylindrical and spherical coordinates, and a combination of this limiter with various acceleration techniques for faster iterative convergence, also constitute our future work. We have observed that, in all our numerical tests including both smooth and discontinuous problems, the cell averages of the unlimited DG solution for the radiative intensity are always nonnegative. Therefore, our "type 1" positivity-preserving limiting procedure, which favors the scaling limiter, uses only the scaling limiting and hence maintains exact conservation. It can be proved that the cell averages of the unlimited DG solution for the radiative intensity should be non-negative for the case without extinction, namely $\sigma_t = 0$, however whether this is true for the general case is unknown and will be carefully studied in the future. In this paper, we have not used any non-oscillatory limiters such as the total variation bounded (TVB) limiters [28, 5, 3] or the weighted essentially non-oscillatory (WENO) limiter [26, 36, 37], hence there are some localized spurious oscillations near the discontinuities in the numerical solution, which are not eliminated by the positivity-preserving limiter if they are not near zero. A combination of the positivity-preserving limiter with the traditional TVB or WENO limiters will also be studied in future work. Finally, we have only considered first order implicit time discretization (backward Euler) in this paper, the extension to higher order implicit methods will be studied in the future as well.

7. Appendix. In this appendix, we will show that the limiter (3.3) can guarantee the original second order accuracy for $I_{m,i}^{(\ell+1)}(x) \in P^1(S_j)$, but may lead to accuracy degeneracy for $I_{m,i}^{(\ell+1)}(x) \in P^2(S_i)$.

We will drop the superscripts and subscripts here as they are irrelevant to our accuracy study, and will simply use a subscript h to denote its relationship to the mesh size. We assume the k-th degree polynomial $I_h(x)$ approximates a smooth function $I(x) \geq 0$ to $(k+1)$-th order accuracy. We only consider the case $\xi = x_{i+1/2}$, i.e. $I_h(x_{i+1/2}) \geq 0$ in (3.3). The limiter is given as

$$\hat{I}_h(x) = \lambda(I_h(x) - I_h(x_{i+1/2})) + I_h(x_{i+1/2})$$

with

$$\lambda = \min\left\{ \left| \frac{I_h(x_{i+1/2})}{I_h(x_{i+1/2}) - z_i} \right|, 1 \right\}, \qquad z_i = \min_{\alpha=1,\ldots,N}(0, I_h(\hat{x}_i^\alpha)).$$

The error between the original polynomial and the modified polynomial, when the limiter is enacted (i.e. when $\lambda < 1$), can be written as follows,

$$|e(x)| = |\hat{I}_h(x) - I_h(x)| = |(\lambda - 1)(I_h(x) - I_h(x_{i+1/2})| = |z_i| \left| \frac{I_h(x) - I_h(x_{i+1/2})}{I_h(x_{i+1/2}) - z_i} \right|.$$

If $I_h(x) \in P^1(S_i)$, then if the limiter is enacted, the negative minimum should appear at the point $x_{i-1/2}$ (since $I_h(x_{i+1/2}) \geq 0$), that is, $z_i = I_h(x_{i-1/2})$. Furthermore, since $I(x_{i-\frac{1}{2}}) \geq 0$, we have $|I_h(x_{i-\frac{1}{2}})| \leq |I_h(x_{i-\frac{1}{2}}) - I(x_{i-\frac{1}{2}})| = \mathcal{O}(h^2)$. Thus we can find

$$|e(x)| = |z_i| \left| \frac{I_h(x_{i-1/2}) - I_h(x_{i+1/2})}{I_h(x_{i+1/2}) - z_i} \right| = |z_i| = \mathcal{O}(h^2).$$

This implies that the limiter (3.3) has maintained the designed second order accuracy if $I_h(x) \in P^1(S_i)$.

If $I_h(x) \in P^2(S_i)$, we will give a counter example to illustrate that the limiter (3.3) may lead to a lower order of accuracy.

Example: Let $S_i = [-h + h^{\frac{3}{2}}, h^{\frac{3}{2}}]$. We assume the smooth function $I(x) = x^2$ and its approximation $I_h(x) = x^2 - h^3$. For the approximation $I_h(x)$, we have the following facts

$$|I(x) - I_h(x)| \leq \mathcal{C}h^3, \qquad I_h(h^{\frac{3}{2}}) = 0, \qquad I_h(-h + h^{\frac{3}{2}}) = \mathcal{O}(h^2).$$

The fact $I_h(h^{\frac{3}{2}}) = 0$ means the limiter parameter $\lambda = \frac{I_h(h^{\frac{3}{2}})}{I_h(h^{\frac{3}{2}}) - z_i} = 0$. Hence the modified function $\hat{I}_h(x) = 0$. Then the error function between the original polynomial and the modified polynomial, evaluated at the left boundary of the cell, is as follows

$$|e(-h + h^{\frac{3}{2}})| = |I_h(-h + h^{\frac{3}{2}}) - \hat{I}_h(-h + h^{\frac{3}{2}})| = |I_h(-h + h^{\frac{3}{2}})| = \mathcal{O}(h^2)$$

which implies the degeneracy of the order of accuracy.

REFERENCES

[1] B.G. Carlson and K.D. Lathrop, *Transport theory - the method of discrete ordinates*, in: H. Greenspan, C.N. Kelber and D. Okrent, editors, Computing Methods in Reactor Physics, Gordon and Breach, New York, 1968, 165-266.

[2] J.C. Chai, S.V. Patankar and H.S. Lee, *Evaluation of spatial differencing practices for the discrete-ordinates method*, Journal of Thermophysics Heat Transfer, 8, 1994, 140-144.

[3] B. Cockburn, S. Hou and C.-W. Shu, *The Runge-Kutta local projection discontinuous Galerkin finite element method for conservation laws IV: the multidimensional case*, Mathematics of Computation, 54, 1990, 545-581.

[4] B. Cockburn, S.-Y. Lin and C.-W. Shu, *TVB Runge-Kutta local projection discontinuous Galerkin finite element method for conservation laws III: one dimensional systems*, Journal of Computational Physics, 84, 1989, 90-113.

[5] B. Cockburn and C.-W. Shu, *TVB Runge-Kutta local projection discontinuous Galerkin finite element method for conservation laws II: general framework*, Mathematics of Computation, 52, 1989, 411-435.

[6] B. Cockburn and C.-W, Shu, *The Runge-Kutta discontinuous Galerkin method for conservation laws V: multidimensional systems*, Journal of Computational Physics, 141, 1998, 199-224.

[7] B. Davison and J.B. Sykes, *Neutron Transport Theory*, Clarendon Press, Oxford, 1957.

[8] W.A. Fiveland, *Discrete-ordinates solutions of the radiative transport equation for rectangular enclosures*, Journal of Heat Transfer, 106, 1984, 699-706.

[9] W.A. Fiveland, *Three Dimensional radiative heat transfer solution by the discrete-ordinate method*, Journal of Thermophysics and Heat Transfer, 2, 1988, 309-316.

[10] A.S. Jamaluddin and P.J. Smith, *Predicting radiative heat transfer in rectangular enclosures using the discrete-ordinate method*, Combustion Science and Technology, 59, 1988, 321-340.

[11] E.W. Larsen and R.E. Alcouffe, *The linear characteristic method for spatially discretizing the discrete-ordinates equations in (x, y)-geometry*, ANS/ENS Joint Topical Meeting, Mathematical Methods in Nuclear Engineering, Munich, FRG, April, 1981.

[12] K.D. Lathrop, *Spatial differencing of the transport equation: Positivity vs. accuracy*, Journal of Computational Physics, 4, 1969, 475-498.

[13] K.D. Lathrop and B.G. Carlson, *Discrete ordinates angular quadrature of the neutron transport equation*, Tech. Report LA-3186, Los Alamos Scientific Laboratory, 1965.

[14] P.D. Lax and B. Wendroff, *Systems of conservation laws*, Communications in pure and Applied Mathematics, 13, 1960, 217-237.

[15] P. Lesaint and P.A. Raviart, *On a finite element method for solving the neutron transport equation*, In Mathematical Aspects of Finite Elements in Partial Differential Equations, C.A. deBoor (Ed.), Academic Press, New York, 1974, 89-145.

[16] E.E. Lewis and W.F. Miller, Jr., *Computational Methods of Neutron Transport*, Wiley-Interscience, New York, 1984.

[17] E. Machorro, *Discontinuous Galerkin finite element method applied to the 1-D spherical neutron transport equation*, Journal of Computational Physics, 223, 2007, 67-81.
[18] N.K. Madsen, *Pointwise convergence of the three-dimensional discrete ordinate method*, SIAM Journal of Numerical Analysis, 8, 1971, 266-269.
[19] N.K. Madsen, *Convergent centered difference schemes for the discrete ordinate neutron transport equations*, SIAM Journal of Numerical Analysis, 12, 1975, 164-176.
[20] P.G. Maginot, J.E. Morel and J.C. Ragusa, *A non-negative moment-preserving spatial discretization scheme for the linearized Boltzmann transport equation in 1-D and 2-D Cartesian geometries*, Journal of Computational Physics, 231, 2012, 6801-6826.
[21] P.G. Maginot, J.C. Ragusa and J.E. Morel, *Discontinuous finite element discretizations for the S_N neutron transport equation in problems with spatially varying cross sections*, Annals of Nuclear Energy, 73, 2014, 506-526.
[22] K.A. Mathews, *Adaptive characteristic spatial quadratures for discrete ordinates neutral particle transport-the slab geometry case*, Transport Theory and Statistical Physics, 19, 1990, 419-458.
[23] M. Mercimek and H.A. Ozgener, *Discontinuous finite element formulations for neutron transport in spherical geometry*, Annals of Nuclear Energy, 64, 2014, 244-255.
[24] J.E. Morel and J.S. Warsa, *An S_N spatial discretization scheme for tetrahedral meshes*, Nuclear Science and Engineering, 151, 2005, 157-166.
[25] G.C. Pomraning, *The Equations of Radiation Hydrodynamics*, Pergamon Press, New York, 1973.
[26] J. Qiu and C.-W. Shu, *Runge-Kutta discontinuous Galerkin method using WENO limiters*, SIAM Journal on Scientific Computing, 26, 2005, 907-929.
[27] W.H. Reed and T.R. Hill, *Triangular mesh methods for the neutron transport equation*, Tech. Report LA-UR-73-479, Los Alamos Scientific Laboratory, 1973.
[28] C.-W. Shu, *TVB uniformly high order schemes for conservation laws*, Mathematics of Computation, 49, 1987, 105-121.
[29] C.-W. Shu and S. Osher, *Efficient implementation of essentially non-oscillatory shock-capturing schemes*, Journal of Computational Physics, 77, 1988, 439-471.
[30] Y. Wang and J.C. Ragusa, *A high order discontinuous Galerkin method for the S_N transport equations on 2D unstructured triangular meshes*, Annals of Nuclear Energy, 36, 2009, 931-939.
[31] T.A. Wareing, *An exponential discontinuous scheme for discrete-ordinate calculations in Cartesian geometries*, in: Joint International Conference on Mathematical Methods and Supercomputing for Nuclear Applications, Saratoga Springs, New York, October 5-9, 1997.
[32] T.A. Wareing, J.M. McGhee, J.E. Morel and S.D. Pautz, *Discontinuous finite element S_N methods on three-dimensional unstructured grids*, Nuclear Science and Engineering, 138, 2001, 256-268.
[33] X. Zhang and C.-W. Shu, *On positivity preserving high order discontinuous Galerkin schemes for compressible Euler equations on rectangular meshes*, Journal of Computational Physics, 229, 2010, 8918-8934.
[34] X. Zhang and C.-W. Shu, *On positivity preserving high order discontinuous Galerkin schemes for compressible Euler equation with source terms*, Journal of Computational Physics, 230, 2011, 1238-1248.
[35] X. Zhang and C.-W. Shu, *Maximum-principle-satisfying and positivity preserving high order schemes for conservation laws: Survey and new developments*, Proceedings of the Royal Society A, 467, 2011, 2752-2776.
[36] X. Zhong and C.-W. Shu, *A simple weighted essentially nonoscillatory limiter for Runge-Kutta discontinuous Galerkin methods*, Journal of Computational Physics, 232, 2013, 397-415.
[37] J. Zhu, X. Zhong, C.-W. Shu and J.-X. Qiu, *Runge-Kutta discontinuous Galerkin method using a new type of WENO limiters on unstructured meshes*, Journal of Computational Physics, 248, 2013, 200-220.